



**KTH Industrial Engineering
and Management**

A mechanical model of an axial piston machine

Rasmus Löfstrand Grip

Licentiate thesis
Department of Machine Design
Royal Institute of Technology
SE-100 44 Stockholm

TRITA – MMK 2009:16
ISSN 1400-1179
ISRN/KTH/MMK/R-09/16-SE
ISBN 978-91-7415-408-5

TRITA – MMK 2009:16
ISSN 1400-1179
ISRN/KTH/MMK/R-09/16-SE
ISBN 978-91-7415-408-5

A mechanical model of an axial piston machine

Rasmus Löfstrand Grip

Licentiate thesis

Academic thesis, which with the approval of Kungliga Tekniska Högskolan, will be presented for public review in fulfillment of the requirements for a Licentiate of Engineering in Machine Design. Public review: Kungliga Tekniska Högskolan, B242, Brinellvägen 81, 114 28 Stockholm, on September 16, 2009, at 13:00.

Abstract

A mechanical model of an axial piston-type machine with a so-called wobble plate and Z-shaft mechanism is presented. The overall aim is to design and construct an oil-free piston expander demonstrator as a first step to realizing an advanced and compact small-scale steam engine system. The benefits of a small steam engine are negligible NO_x emissions (due to continuous, low-temperature combustion), no gearbox needed, fuel flexibility (e.g., can run on biofuel and solar), high part-load efficiency, and low noise. Piston expanders, compared with turbines or clearance-sealed rotary displacement machines, have higher mechanical losses but lower leakage losses, much better part-load efficiency, and for many applications a more favourable (i.e., lower) speed. A piston expander is thus feasible for directly propelling small systems in the vehicular power range. An axial piston machine with minimized contact pressures and sliding velocities, and with properly selected construction materials for steam/water lubrication, should enable completely oil-free operation. An oil-free piston machine also has potential for other applications, for example, as a refrigerant (e.g., CO₂) expander in a low-temperature Rankine cycle or as a refrigerant compressor.

An analytical rigid-body kinematics and inverse dynamics model of the machine is presented. The kinematical analysis generates the resulting motion of the integral parts of the machine, fully parameterized. Inverse dynamics is applied when the system motion is completely known, and the method yields required external and internal forces and torques. The analytical model made use of the “Sophia” plug-in developed by Lesser for the simple derivation of rotational matrices relating different coordinate systems and for vector differentiation. Numerical solutions were computed in MATLAB. The results indicate a large load bearing in the conical contact surface between the mechanism’s wobble plate and engine block. The lateral force between piston and cylinder is small compared with that of a comparable machine with a conventional crank mechanism.

This study aims to predict contact loads and sliding velocities in the component interfaces. Such data are needed for bearing and component dimensioning and for selecting materials and coatings. Predicted contact loads together with contact geometries can also be used as input for tribological rig testing. Results from the model have been used to dimension the integral parts, bearings and materials of a physical demonstrator of the super-critical steam expander application as well as in component design and concept studies.

Keywords: Multi-body mechanical model, axial piston, Z-shaft, wobble plate, Sophia

Preface

This text covers the major part of the work I've conducted from November 2006 to July 2009 at the Department of Machine Design at the Royal Institute of Technology, Stockholm, Sweden and in collaboration with the Swedish company Ranotor. A large portion of the time was devoted to understanding and trying to capture the kinematics and dynamics of the axial piston machine that is the subject of my research. Much effort has also been put in trying to figure out and supervising meaningful student's projects that would incorporate my results in useful applications and sub-systems of the axial piston machine and the steam-engine system as a whole. The engagement of clever and creative students in the research has greatly extended the domain covered.

Ove Platell and Peter Platell at Ranotor have of course posed an invaluable support and a source of great knowledge and enthusiasm. The support and input also extends to my excellent supervisors Jan-Gunnar Persson, Ulf Olofsson and Ulf Sellgren and my colleagues at the department. I would like to give a special thanks to Anders Söderberg and Klas Schjelderup whom respectively contributed to my theoretical and practical understanding of mechanics and machine design.

Stockholm, August 2009

Rasmus Löfstrand Grip

List of appended papers

This thesis consists of a summary and the following three appended papers:

Paper A

Grip, R., "Axial piston machine kinematics," OST Proceedings, 2007, Tallinn, Estonia.

Paper B

Grip, R., Persson, J-G., "Describing a mechanical model of a novel axial piston type steam expander ," OST Proceedings, August 2008, Tallinn, Estonia.

Paper C

Grip, R., "A dynamical model of an axial piston machine," Submitted to Journal of Applied Mechanics, ASME, August 2009.

Division of work between authors

The work presented in this thesis was initiated and supervised by Jan-Gunnar Persson, Ulf Olofsson and Ulf Sellgren.

Paper A

Rasmus Löfstrand Grip, author.

Paper B

Rasmus Löfstrand Grip, main author.

Paper C

Rasmus Löfstrand Grip, author.

Contents

1	Introduction.....	1
2	State of the art	2
3	Research questions.....	14
4	Model.....	15
5	Results.....	42
6	Summary of appended papers.....	45
7	Discussion, future research and conclusions	46
8	Associated work	47

Appended papers

- A. Axial piston machine kinematics
- B. Describing a mechanical model of a novel axial piston type steam expander
- C. A dynamical model of a axial piston machine

1 Introduction

A device that is used to convert heat to mechanical work is defined as a heat engine. They receive heat from a high-temperature source, indifferent of the primary energy source used to generate this heat. Part of the heat is converted to mechanical work, whereas the remaining heat is rejected to a low-temperature sink. The operation is cyclical or continuous [1]. Examples of continuous heat engines are gas turbines and steam turbines. Examples of cyclical heat engines are internal combustion engines (ICE) such as the diesel and otto (gasoline) engine and external combustion engines (ECE) such as steam piston engines and Stirling engines. In order to convert the heat to work some kind of expander is used. Depending on the power range, fuel supply, environmental restrictions etc. of the application, different thermal cycles and expander types are applicable and feasible.

During the oil-crisis of the 1970's, the automotive industries turned their attention to alternative engine concepts, e.g. gas turbines and steam engines. Poor design solutions like bulky condensers with energy inefficient fans, later led the majority of the researchers to abandon the steam engine as a concept [2]. Today steam cycles (Rankine cycle with water as working medium, or Organic-Rankine cycle with refrigerant as working medium) and Stirling cycles are employed in micro-CHP (Combined Heat and Power) where fuel is used to power a small scale heat engine. The engine shaft power is used to generate electricity and the rejected low temperature heat is used for heating living spaces [3]. Another steam engine application is in a bottoming cycle where waste heat from an industrial process or internal combustion engine is recovered and the shaft power is used to generate electricity or to directly contribute to the traction of a vehicle.

This thesis is on the subject of modelling a rigid body mechanical model of an axial piston type machine. The overall aim of this research is to design and construct an oil-free piston expander demonstrator as a first step to realizing an advanced and compact small-scale steam engine system. Several student projects and master theses have also been carried out as sub-projects, some utilizing the results from the mechanical model presented in this thesis, together with input from researchers and mechanical engineers involved in the project and the vast amount of knowledge and experience gathered by Ranotor. The student projects comprise concept studies on waste heat recovery and solar thermal power, advanced oil-free test rigs for the inlet valve and a support system for the hydrostatic lubricated seals, finite element analysis of the integral parts of the steam expander and multi-body system (MBS) simulations and computational fluid dynamics simulations. Results from the student projects have been used within this project and these sub-projects are briefly presented in the chapter 8, "Associated work".

The limitations of the mechanical model presented in this thesis can be divided into application limitations and model limitations. The application limitation besides the specific type of piston machine is primarily an aspect of power range, where the “small power output” is regarded (a range below 1000 kW). Above this power range, other machines than the reciprocating piston type are more suitable [4][5]. Regarding the model limitations, the parts of the machine are assumed to be rigid bodies. Further, the dynamics of the machine is modelled in an inverse dynamics fashion, though this does not exclude running forward dynamics simulations within the same model.

2 State of the art

2.1 Steam engines

Steam engines have favourable characteristics for many areas of application. External combustion enables great flexibility concerning possible fuel sources, which is beneficial from an energy supply perspective. The fuel flexibility includes liquids and gases such as gasoline, diesel oil and ethanol; solid fuel such as waste products from the agricultural industry; concentrated heat such as solar collectors or waste heat from internal combustion engines or industrial processes. Further, the combustion can, preferably with the aid of buffers in the steam engine system, be continuous and fairly constant even for cases where the load is varying. The combustion temperature is low compared to ICE engines. This enables very low or zero-emission of NO_x and particulates [6].

The torque and efficiency characteristics are also favourable for many applications such as automotive, due to the possibility for high part load efficiency by means of filling control of piston expanders [6].

2.1.1 The Rankine cycle

The Carnot cycle is theoretically the most efficient thermodynamic cycle, but impractical to realize. Instead, the Rankine cycle is considered to be the ideal vapour power cycle. The four state changes of an ideal (loss-free) Rankine cycle are (see Figure 1):

- 1-2 Liquid pressurizing in a feed pump (\dot{W}_{in})
- 2-3 Continuous heat addition in boiler (\dot{Q}_{in})
- 3-4 Isentropic expansion in an expander (\dot{W}_{out})
- 4-1 Continuous heat rejection in a condenser (\dot{Q}_{out})

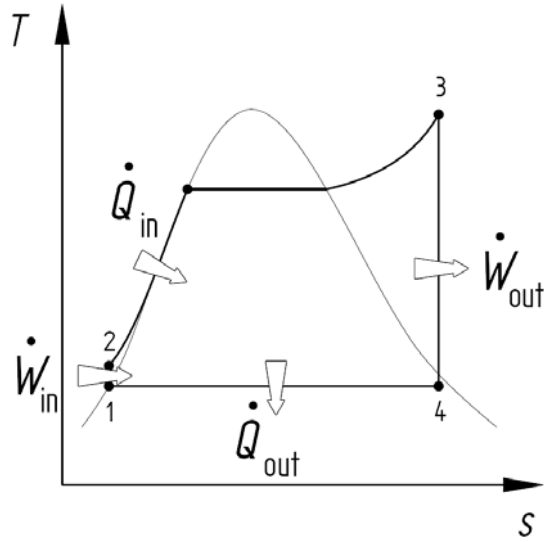


Figure 1 – The ideal Rankine cycle presented in a entropy vs. temperature diagram. An increase in energy of the system is done to the system by \dot{W}_{in} at 1-2 (pressurizing in feed pump) and \dot{Q}_{in} at 2-3 (addition of heat in burner). A decrease in energy is done on the system by \dot{W}_{out} at 3-4 (expansion in expander) and \dot{Q}_{out} at 4-1 (heat rejection in condenser).

The thermal efficiency and therefore the amount of possible performance of mechanical work per input energy are related to the difference between admission (high) and condenser (low) pressure and temperature [1].

2.1.2 Contemporary steam engines

Today, there is an emerging interest and market for small to large-scale commercial steam engines. Typical applications are stationary units, e.g. CHP (Combined Heat and Power), and waste heat recovery and bottoming cycle, but mobile and automotive applications are also of great and growing interest. In stationary waste heat recovery and cogeneration plants, the exhaust heat from a gas turbine, from an industrial process, or from an internal combustion engine is used to produce steam which together with a steam expander and possibly an electric generator generates mechanical power and or electricity. Examples of suppliers of stationary steam engines are Spilling Energie Systeme (piston steam engines and steam turbines) and Siemens Power Generation (steam turbines). For mobile applications, Cyclone Power Technology and Amovis GmbH are investigating small scale piston steam engines of radial and axial piston type configurations.

The bottoming cycle principle is depicted in Figure 2.

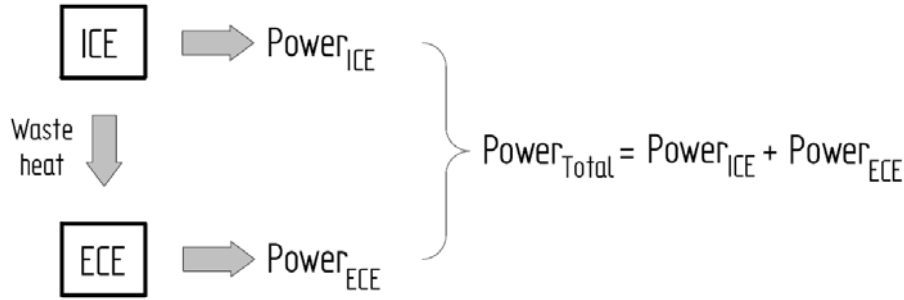


Figure 2 – Principle diagram for a bottoming or waste heat recovery cycle. Waste heat from the exhaust of an internal combustion engine is used to generate additional mechanical power via an external combustion engine (i.e. via a heat recovery steam generator and a steam engine system). The total power of this subsystem exceeds the power generated by the ICE.

2.2 Expander types

To convert heat to mechanical work some type of expander has to be utilized. Different kinds of expanders are suitable concerning efficiency and mechanical aspects, depending on the application, i.e. power range. Generally there is a characteristic optimum peripheral velocity (tip speed) u (or mean piston velocity for reciprocating machines), for every type of positive displacement machine, determined by their inherent leakage and throttling losses [7]. This optimal tip speed is fairly independent of the machine size and virtually constant for a uniform specific type of machine. Also for turbo (dynamic) machines there is a fairly size independent optimum tip speed, in this case primarily determined by vane geometry (the “specific speed” parameter for turbo machines) [4]. Thus, from the kinematic relation $u = \pi \cdot D \cdot n$, the optimal shaft speed n becomes dependent of the machine size (rotor diameter) D (Figure 3).

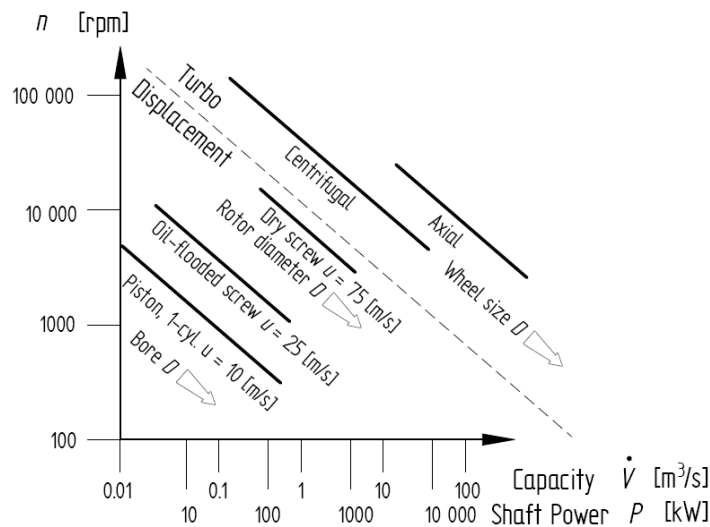


Figure 3 – Optimal shaft speed and volume flow relations for positive displacement and turbo machines. Power scale valid for air compression duty (after [4]). As seen, the closest match on shaft speed in applications such as the automotive application corresponds to the optimal shaft speed of piston machines.

In general turbines operate at a very high peripheral speed (some 200 - 300 m/s) for optimum efficiency, which means that the shaft speed will be very high for small turbines in the vehicular power range. Complex gearing will then be required for a turbine to be used for vehicle traction. Also clearance sealed rotary displacement machines (e.g. the Lysholm-screw) have relatively high optimal peripheral speed (typically 80 - 120 m/s for a dry – i.e. non-injected - screw machine) which is determined from the balance between leakage losses in clearances and throttling losses in inlet and outlet ports [7]. Like turbines, also clearance sealed rotary displacement machines have poor performance at low speed, due to higher influence of internal leakage at low speed.

Piston machines have, due to friction losses in piston rings, crank pins, crankshaft bearings and valve train, higher mechanical losses than turbines or clearance sealed rotary displacement machines. However, a piston steam engine experiences considerably lower relative mechanical losses than a comparable internal combustion engine, due to the generally higher portion of useful performance of mechanical work, i.e. higher cylinder mean pressure at full load (i.e. "thicker" indicator diagram over one piston stroke) in a steam engine. They also have substantially lower leakage flows (blowby) because of active seal elements, i.e. piston rings. This is the explanation of piston expanders and piston compressors good efficiency also at low speed [5].

2.3 Steam piston engines with filling control

The torque and efficiency characteristics of a steam piston engine are favourable for many applications such as automotive, due to the high part load efficiency of a steam engine with filling control. A piston steam engine will deliver maximum torque at zero rpm. By filling control, i.e. admission over a variable part of the stroke, there will be internal expansion at part load and hence maximum efficiency at part load, while higher torque but lower efficiency is obtained by “full pressure” operation, i.e. filling during the entire stroke [5][6], as illustrated in Figure 4.

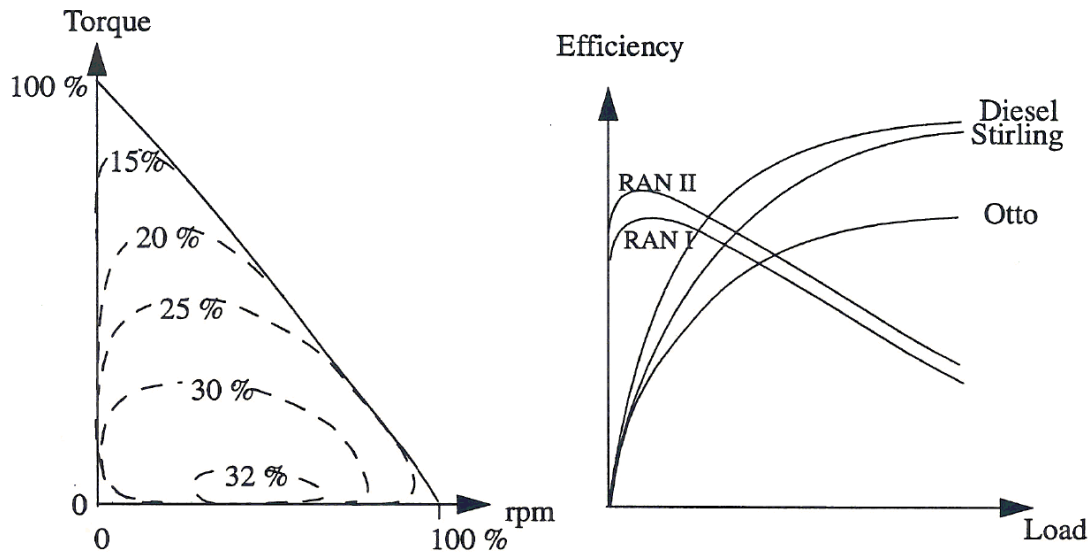


Figure 4 – Illustration of the torque characteristics and efficiency of a filling controlled piston steam engine, and efficiency vs' load for different engines [6]. A piston steam engine gives maximum torque at zero rpm and a filling controlled piston expander offers its highest efficiency at part load (which is the significant load in many applications, such as the majority of automotive application). The left graph illustrates the performance map with torque characteristics together with efficiency levels. The graph at the right-hand side illustrates the efficiency vs. load of two steam engine configurations (RAN I and RAN II, which differ in admission temperature and pressure) and the otto, stirling and diesel engines.

2.4 Axial piston steam expander

The pistons of an axial piston machine are placed centred around the engine shaft and the reciprocating motions of the pistons are in the symmetry direction of the engine shaft. The pistons are connected to piston rods which in turn act upon some kind of tilted plate (Figure 5).

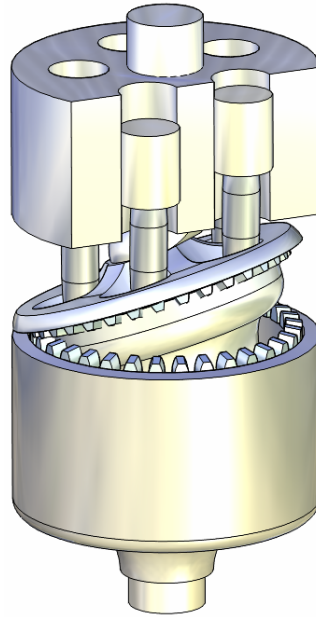


Figure 5 – An axial piston type expander. As seen, the pistons (here five) are placed centred around the engine shaft and force the tilted plate (here wobble plate) to move via piston rods. The tilted plate in turn forces the engine shaft to rotate.

Depending on the configuration, the tilted plate has different names; e.g. bent axis, swash plate and wobble plate. The tilted plate is either part of the engine shaft or jointed with some relative degree of freedom to the engine shaft. If the tilted plate is part of the engine shaft and the piston rods are rigidly connected to the tilted plate, the cylinder head has to rotate with the engine shaft. This configuration is called bent axis and can have a fixed or variable (adjustable) displacement. If the piston rods slide upon the tilted plate, thus enabling a non-rotating cylinder head, the configuration is called swash plate. There also exists a hybrid between the bent axis and swash plate configuration which is called swash plate or wobble plate with Z-shaft interchangeable. The hybrid has a tilted plate that is rigidly connected to the engine shaft, but with yet another tilted plate upon the engine shaft plate. In between the two plates is some kind of bearing that allows for relative rotation about the symmetry axis. Yet another configuration is when the piston rods are jointed to a tilted plate which is cylindrical or revolute jointed to the engine shaft, which in turn has a tilted part. In this configuration, the tilted plate is called wobble plate and the engine shaft is called Z-shaft and the cylinder head is non-rotating. The wobble plate has to be synchronized to the machine casing in order to prevent rotation to and establish a pure nutating motion. This solution lowers the lateral loads between piston and cylinder liner, since the piston rods don't slide upon the tilted plate and no such friction force component from sliding is transferred to the contact between piston and cylinder liner. The different axial piston machine concepts are illustrated in Figure 6.

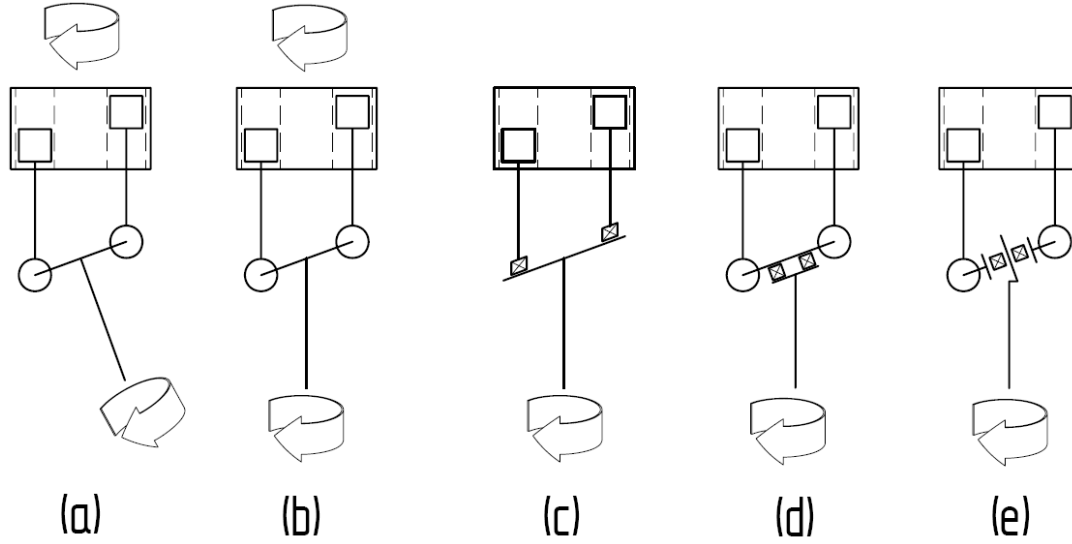


Figure 6 – Axial piston type engines of different configurations: (a) Bent axis with variable displacement, (b) Bent axis with fixed displacement, (c) Swash plate (here with fixed displacement), (d) Hybrid configuration, interchangeable named swash plate and wobble plate with Z-shaft, (e) Wobble plate with Z-shaft. As illustrated, the two bent axis configurations require a rotating cylinder head.

2.5 Historical and contemporary axial piston machines

There are both contemporary and historical examples of axial piston machines with wobble plate mechanism. Closest related contemporary commercial products are the wobble plate AC-compressors by Sanden and other suppliers. Early historical examples of axial piston machines with wobble plate and Z-axis that have been in experimental use, but not commercialised, are internal combustion engines in buses and airplanes [8].

2.6 The RAN-concept

The RAN-concept is thoroughly described in [6], and will here only be briefly described (illustrated in Figure 7). A power cycle with CO_2 as working media was investigated by Chen [9]. Conclusions are that the CO_2 cooling and power combined cycle is energy efficient in the automobile application.

The system realizes a Rankine cycle with the additional capability of transferring heat to a steam buffer. The concept consists of three subsystems; the steam generating system, the expander system and the condenser system. The steam generating system comprises a burner, a steam generator and a steam buffer (which are aided by pumps). The expander system consists of an axial piston type expander with some type of variable valve mechanism and a mechanical interface (output shaft) to the external system. The condenser system comprises the condenser and a condenser buffer. The RAN expander operates between the steam admission state 500 °C, 250 bar and the condenser state 80-130 °C, 0.5-3 bar.

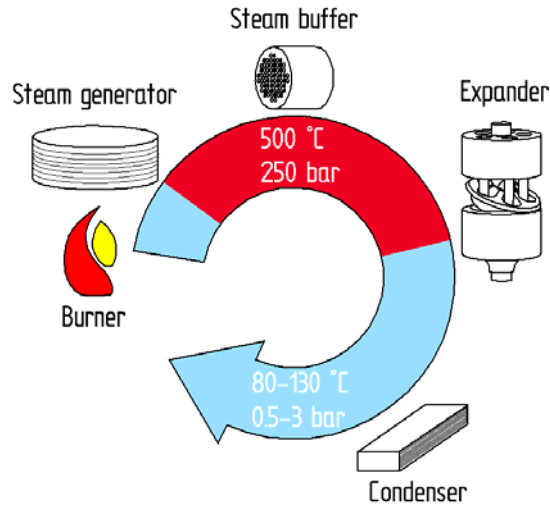


Figure 7 – A schematic representation of the components of the subsystems in the RAN-concept. The three subsystems are the steam generating system (burner, steam generator and steam buffer), the expander system (expander plus valves and mechanical interface to the environment) and the condenser system (comprising condenser and condenser buffer). The steam generating system generates and controls steam at 500 °C and 250 bar. After the expander, the condenser state is 80-130 °C and 0.5-3 bar.

The steam buffer performs two tasks; it enables peak-shaving which thus (ideally) enables continuous combustion at constant power and it also allows for regenerative braking via transforming some of the kinetic energy to pressurized steam. A theoretical and experimental study on a thermal energy storage device utilizing hot water was conducted by Naqvi [10] which showed the capability to store and regenerate thermal energy. Although the experimental results from the test rig differed from theoretical predictions, Naqvi encourage continued research.

If equipping an average sized car (gross weight of 1000 kg and an aerodynamic drag area of 55 dm²) with a RAN-engine dimensioned such that it operates at part load in the significant load range, Platell [11] judges an over all (fuel to speed) efficiency of 20-25% feasible. In an urban driving cycle (Federal Driving Cycle Urban, FDC-U), this would correspond to 0.43 litres of diesel fuel per 10 km, and at a highway driving cycle (Federal Driving Cycle Highway, FDC-H) it would consume 0.40 litres of diesel fuel per 10 km. The power output of such a configuration would be approximately 150 kW.

2.7 The design concept

From a design point of view, there are many possibilities to fulfil the motion of the integral parts of the machine, which has a direct effect on the resulting contact loads and velocities. The concept at hand (Figure 5) comprises a wobble plate, which together with piston rods act as intermediary components in transforming the reciprocating motion of the pistons to rotation of the engine shaft. One revolution of the engine shaft results in one full cycle for each piston, which is illustrated Figure 8.

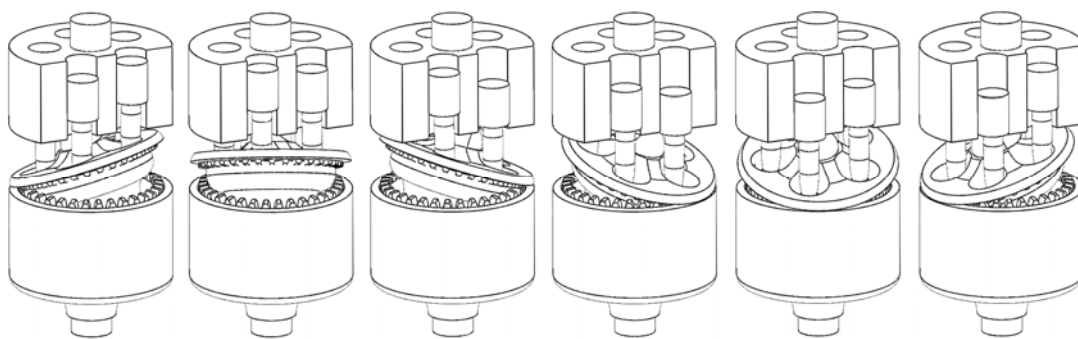
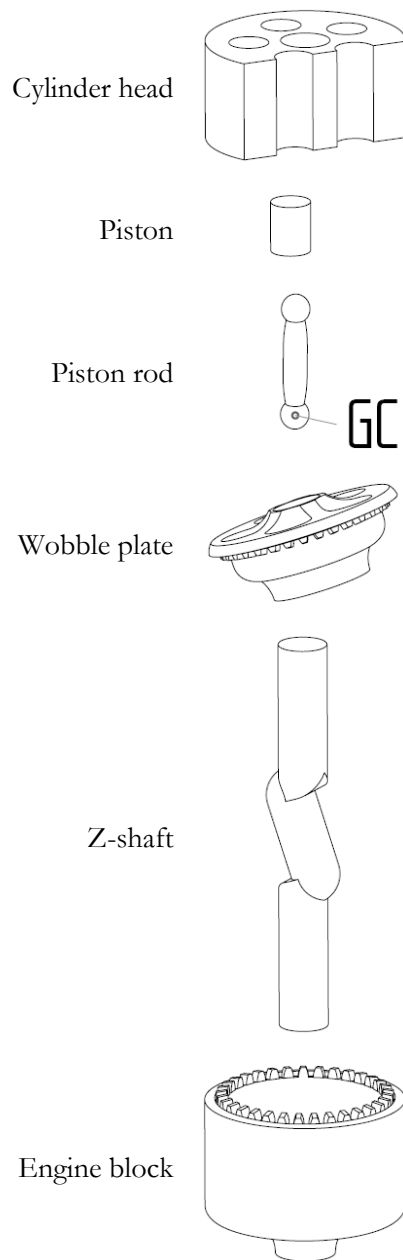


Figure 8 – The design concept. The series of snapshots shows one revolution of the engine shaft.

The integral parts of the machine are presented in Table 1.

Table 1 – The names and schematic geometries of the integral parts of the machine. The geometric centre of the lower ball joint of the piston rod, abbreviated “GC” is of great importance and discussed further in the model chapter.



The wobble plate is connected to the engine shaft called the Z-shaft from its geometrical form, where the mechanical work performed by the machine is taken out. Further, the wobble plate has to be synchronized in order to establish a pure nutating motion. This synchronization can be realized in many ways. Examples of different solutions are the so called “frying pan” mechanism where a connecting pin from the wobble plate runs in a slot in the engine block, the “fishplate” mechanism similar to the “frying pan” solution,

or by coupling the wobble plate and engine block via a gear. In the model presented in this thesis, an equivalent to the gear solution is utilized. There is also great freedom in preventing the wobble plate from translating axially along the Z-shaft. One such solution is to mount the wobble plate upon a tilted plate connected to the engine shaft, with axial (conical) bearings in-between (the hybrid swash/wobble plate solution seen in (d) in Figure 6). Another solution is to form a cone-to-cone contact (preferably with a slight crowning) between wobble plate and engine block (see Figure 9). In the model presented in this thesis, the latter solution is utilized. This enables the conical contact surfaces to carry the major part of the axial load exerted upon the wobble plate from the gas forces, i.e. steam expanding in the cylinders.

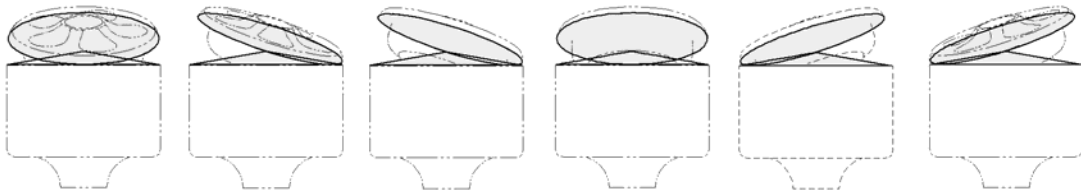


Figure 9 – The rolling without sliding of the wobble plate upon the engine block.

Further, if the geometrical centres of the lower ball joints of the piston rods, GC, are placed in the so called wobble plane (Figure 10), the trajectory of these points form a double closed loop with a constant radius from the central axis and a pure sinusoidal vertical translation. If the piston is placed above the centre of the double closed loop, the piston itself is subjected to a pure sinusoidal motion with the same amplitude. Complete balancing of the machine by counterweights will then be possible.

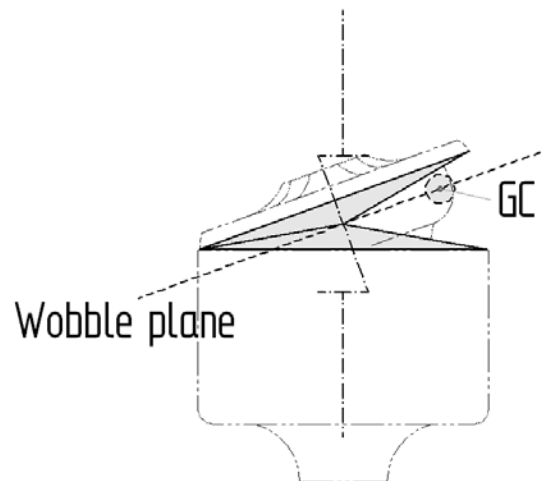


Figure 10 – The placing of “GC” in the wobble plane reduces the motion of the piston to a pure sinusoidal translation.

There are different degrees of freedom in relative motion between the integral parts of the machine, which must be realized by corresponding types of joints. Figure 11 illustrates the joints (and Table 2, chapter 4, the names of these later used in the model of the machine).

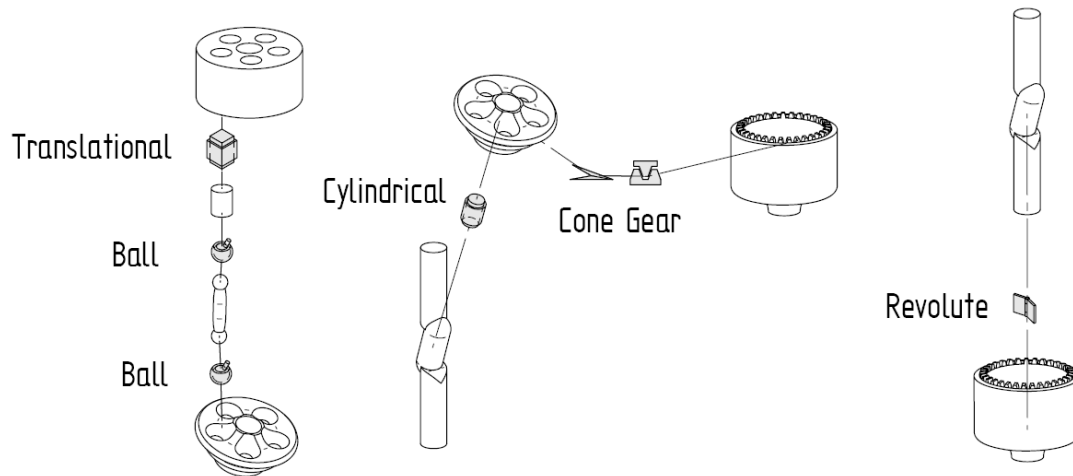


Figure 11 – The joints connecting the integral parts of the machine; translational joint connecting cylinder head and piston, ball joint connecting the piston and piston rod, ball joint connecting the piston rod and the wobble plate, cylindrical joint connecting Z-shaft and wobble plate, cone joint connecting the wobble plate and engine block, gear joint connecting the wobble plate and engine block, revolute joint connecting the Z-shaft and engine block.

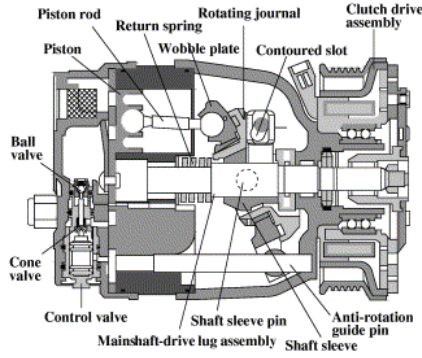
2.8 Motives to constructing a mechanical model

A kinematical and an inverse dynamical model, together with the kinematic analysis, will predict the contact loads and the relative velocities in the interfaces of interest. Contact loads are vital for dimensioning of the bearings, for dimensioning of components and selection of materials and coatings, as well as in supporting the understanding of the force and torque distribution throughout the machine. Predicted contact forces from the rigid body model together with contact geometries can be used as input to calculate contact pressure. It also enables for a finite element analysis of single components to predict stress levels and elastic deflections which incorporates transmitted loads from both applied loads and inertial loads upon the component interfaces (with the inherent errors introduced by such a simplification). Also, the predicted contact forces and relative velocities can be used as input for tribological rig testing.

2.8.1 Related models

The kinematics of this kind of wobble plate engine has been analyzed by Lang [12]. The results from the model by Lang were verified by Grip, Paper A. As far as the author is aware of there are no existing directly applicable dynamical models of wobble plate engines with Z-shaft, gear synchronisation and load carrying conical surfaces, though there are examples of dynamic models of similar wobble plate machines [13][14], see Figure 12. The machine modelled by Tian et al. [13] is of the “frying pan” mechanism

(see (a) in Figure 6), and the model by Pedersen [14] is of the “fishplate” mechanism (see (b) in Figure 6).



(a)

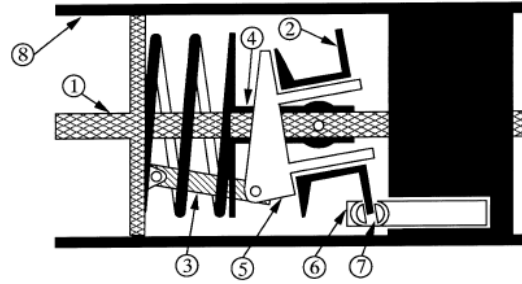


Figure 1. 2D picture of the compressor: 1. the shaft; 2. the wobble plate; 3. the fishplate; 4. the spring handle; 5. the inclined plate; 6. one of seven pistons; 7. seven ball bearings; 8. the ground show as a cylinder around the compressor.

(b)

Figure 12 – Two axial piston type wobble plate machines found in literature. Illustration (a) depicts a so called “frying pan” mechanism where the wobble plate is synchronized via a guiding pin [13]. Illustration (b) depicts a so called “fish plate” mechanism where the wobble plate is synchronized in a similar manner to the “frying pan” mechanism [14].

3 Research questions

This thesis concerns developing a rigid body mechanical model of an axial piston type machine. The integral parts of the machine are assumed to be rigid bodies. The dynamics of the machine is modelled in an inverse dynamics fashion, though this does not exclude running forward dynamics simulations within the same model. A generic and compact matrix-based analytical approach has been applied, for determination of all internal forces.

The research questions are:

- How can contact loads and relative velocities between the integral parts of the machine be determined?
- Will pure harmonic motion of the pistons be achievable?
- Can the inertias of the integral parts of the machine be completely out-balanced by means of proper selection of geometric parameters and by mounting dead-weights upon the Z-shaft?

4 Model

This chapter briefly summarises the construction of the analytical kinematical and inverse dynamical rigid body model of the axial piston type machine with wobble plate and Z-shaft, as presented in detail in the appended papers. The kinematics of the integral parts of the machine is derived. Thereafter, the constraints of the integral joints of the machine are applied to the bodies, as well as the known applied loads (steam pressure and gravity), which together with component mass and mass moment of inertia form the Euler equations. A simplified model of the steam pressure as a function of the Z-shaft angle of rotation is then described and acts on the system of bodies as a known applied force upon the pistons. Numerical computation of result parameters (contact loads and external shaft torque) requires input data on a number of parameter sets, which are presented and given “default” values (if not stated otherwise).

The chapter “Balancing of inertias” covers the topic of reducing the external constraint loads to only carrying the dead weight of the machine and to absorb the output shaft torque. This reduces the machine to a completely out-balanced or “vibration free” mechanism.

The kinematic and dynamic model was implemented in the mathematical computer program Maple with the aid of the “Sophia” plug-in by Lesser [15], which allowed for analytical modelling, simplified derivation of rotational matrices and the differentiation of vectors. Numerical solutions and graphs have been calculated in the computer program Matlab.

Part of the results on contact loads and relative velocities presented in this thesis was used to construct a physical demonstrator of the machine [16]. The integral components, i.e. piston-piston rod, wobble plate, Z-shaft, engine block, cylinder head, rotating valve, bearings and materials were dimensioned and selected to meet the requirements from a machine with a steam admission pressure of 250 bar and temperature of 450 °C, with a rotational speed of 6000 rpm where possible. During the design of the machine some requirements were not met in order to progress with the actual construction. This led to the usage of some results not valid for the actual demonstrator, but since the machine won’t operate at full admission pressure the dimensioning will not inhibit the function as a demonstrator. The results presented in this thesis are the results that should be valid for the final design. The integral parts are made mass-less to eliminate the influence of inertias since these were considered mostly to reduce the contact loads.

4.1 Kinematical model

The position and orientation vectors are derived by defining body-fixed coordinate systems to the Z-shaft and the wobble plate. Subjecting the contact between wobble plate and Z-shaft to a no-slip condition, the relation describing the relative rotation between Z-shaft and wobble plate is derived. Thereafter, the position vector of the piston is derived with a closed-loop geometric constraint. Defining a general body-fixed coordinate system for a piston rod, together with an intermediate coordinate system, the constraint of ball-jointing the piston rod to the wobble plate and the associated piston gives the relation describing the relation between the body fixed coordinate system of the piston rod and the inertial coordinate system.

Influence of the radial position of the piston/cylinder centre is investigated. If the piston is placed at a certain radius, the vertical piston motion is pure sinusoidal. This also applies to the vertical motion of the piston rod. Further, taking the sum of the lateral accelerations of the piston rods gives a vector of zeros as a result. This implies that the resulting inertia of the piston rods from the centre of mass accelerations is completely self balanced-out.

4.1.1 Coordinate systems

The relative rotations between the coordinate systems are stated in Eq. 1. The coordinate systems initially defined are presented in Figure 13 and Figure 14.

$$\begin{aligned}
 &N \text{ space fixed} \\
 &N \rightarrow Z \text{ with } \varphi_1 \\
 &Z \rightarrow T \text{ with } \alpha \\
 &T \rightarrow W \text{ with } \varphi_2 \\
 & \\
 &N \rightarrow \text{Pr 1 with } \gamma \\
 &\text{Pr 1} \rightarrow \text{Pr 2 with } \beta
 \end{aligned}
 \tag{Eq. 1}$$

Where φ_1 , φ_2 , γ and β are dependent on time

And where a is defined as a constant

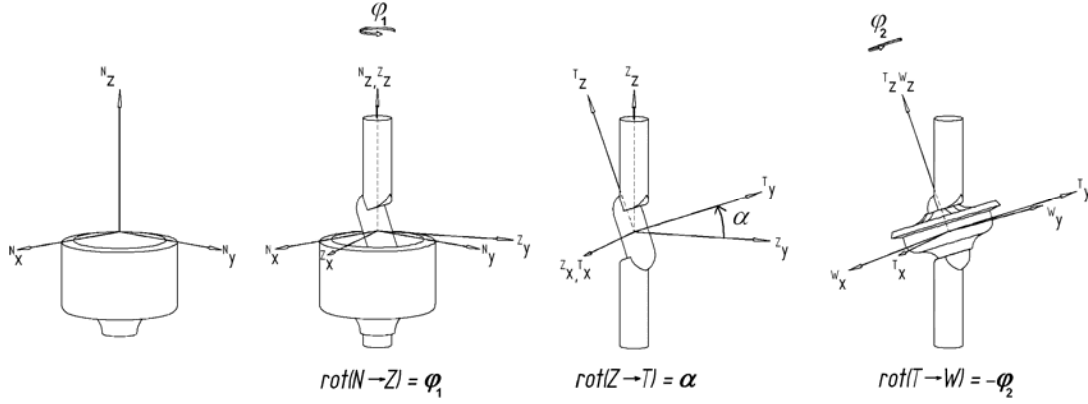


Figure 13 – The coordinate system ‘N’ constitutes a space fixed coordinate system. The coordinate system ‘Z’ is configured by rotation of φ about ‘N’ z -axis. Coordinate system ‘T’ is configured by rotation of α about ‘Z’ x -axis. Coordinate system ‘W’ is configured by rotation of $-\varphi$ about ‘T’ z -axis.

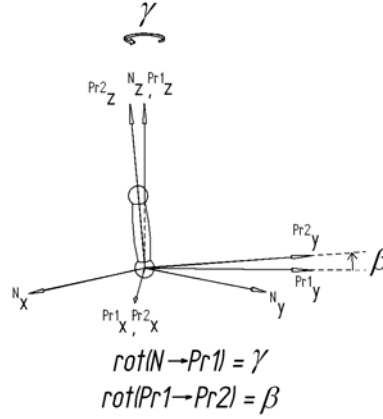


Figure 14 – Coordinate system ‘Pr1’ is configured by rotation of 2φ about ‘N’ z -axis. Coordinate system ‘Pr2’ is configured by rotation of β about ‘Pr1’ x -axis.

There are transformation matrices from each coordinate system to the other, denoted $R_{A \rightarrow B}$ where the suffix $A \rightarrow B$ imply the transform of coordinate system ‘B’ seen from ‘A’. The rotational velocity and rotational acceleration is denoted $\bar{\omega}_{A \rightarrow B}$ and $\dot{\bar{\omega}}_{A \rightarrow B}$

4.1.2 Wobble plate

As mentioned in the introductory chapter, the wobble plate rolls without sliding upon the engine block in a cone-to-cone contact. This constitutes a no-slip condition at the point of contact between wobble plate and engine block, i.e. a gear contact with the pitch radius somewhere on the contact line between the two cones. The apexes of the two cones meet at one (virtual) point and the two cones are of the same pitch. The point of contact is defined by two vectors; one body fixed with the wobble plate defined by the vector \bar{r}_w and one body fixed with the engine block defined by the vector \bar{r}_c . A no-slip condition is a non-holonomic constraint, the time derivatives (i.e. velocities) of the two vectors shall equal, see Figure 15. This gives the equations Eq. 2.

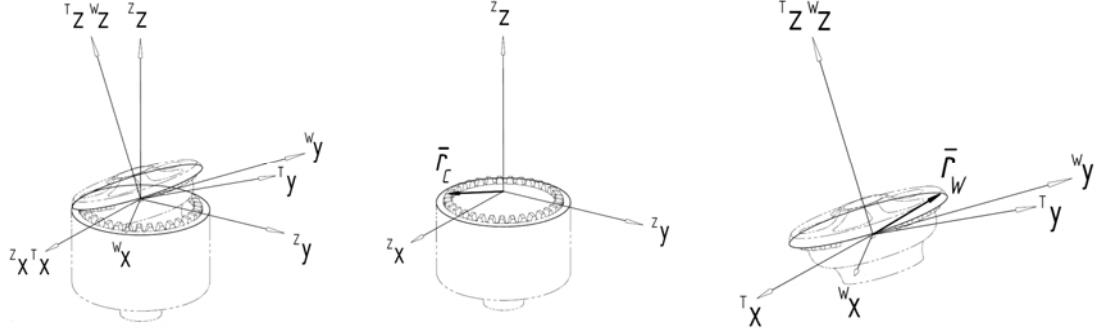


Figure 15 – The leftmost image shows the engine block and the wobble plate with gear synchronization in dashed lines together with the relevant coordinate systems ('Z' being the Z-shaft body fixed coordinate system, 'T' also Z-shaft fixed but tilted by a round the Zx -axis and 'W' body fixed to the wobble plate and rotated an arbitrary angle φ_2 round the Tx -axis). The middle image shows the vector \bar{r}_c pointing to the specified contact point between wobble plate and engine block. The rightmost image shows the vector \bar{r}_w pointing on one point along the on the pitch radius of the gear of the wobble plate.

$${}^Z[\bar{r}_c] = {}^Z[0 \quad -R_w \quad -h_w] \Rightarrow \dot{\bar{r}}_c = \frac{d}{dt}({}^N\bar{r}_c)$$

$${}^T[\bar{r}_w] = {}^T[0 \quad -R_w \quad -h_w] \Bigg\{ \bar{\omega}_{T \rightarrow W} \Bigg\} \Rightarrow \dot{\bar{r}}_w = \bar{r}_w \times \bar{\omega}_{T \rightarrow W}$$

$$\Rightarrow \{no - slip\} \Rightarrow \dot{\bar{r}}_c = \dot{\bar{r}}_w \Rightarrow \dot{\bar{r}}_c - \dot{\bar{r}}_w = 0 \Rightarrow$$

Eq. 2

$$\Rightarrow \begin{bmatrix} R_w \cos(\varphi_2) \dot{\varphi}_1 + R_w \cos(\varphi_2) \dot{\varphi}_2 \\ -R_w \sin(\varphi_2) \dot{\varphi}_1 - R_w \sin(\varphi_2) \dot{\varphi}_2 \\ 0 \end{bmatrix} = \begin{bmatrix} 0 \\ 0 \\ 0 \end{bmatrix} \Rightarrow \begin{bmatrix} \dot{\varphi}_2 = -\dot{\varphi}_1 \\ \dot{\varphi}_2 = -\dot{\varphi}_1 \\ 0 \end{bmatrix}$$

Thus, the rotation of the wobble plate is the exact opposite of the rotation of the Z-shaft. Henceforth φ_1 is denoted φ and φ_2 is denoted $-\varphi$ (Eq. 3).

$$\varphi_1 \equiv \varphi, \quad \varphi_2 \equiv -\varphi$$

Eq. 3

4.1.3 Lower ball joint of piston rod, GC

The position vector \bar{r}_{GC} of the lower ball joint GC between piston rod and wobble plate is used in the derivation of the positions of piston and piston rod (see \bar{r}_{GC} in Figure 18).

It is defined in the wobble plate body fixed system (see Eq. 4) and if placed in the wobble plane, the trajectory forms a double-closed curved eight shape. The vertical displacement is purely sinusoidal and the lateral displacement forms a perfect circle.

$${}^w[\bar{r}_{GC}] = {}^w[0 \quad R \quad 0] \quad \text{Eq. 4}$$

\bar{r}_{GC} transformed to the inertial (“ground”) coordinate system ‘N’ (Eq. 5) yields the double-closed 8-shaped loop with a sinusoidal vertical displacement and circular lateral trajectory, see Figure 16 and Figure 17.

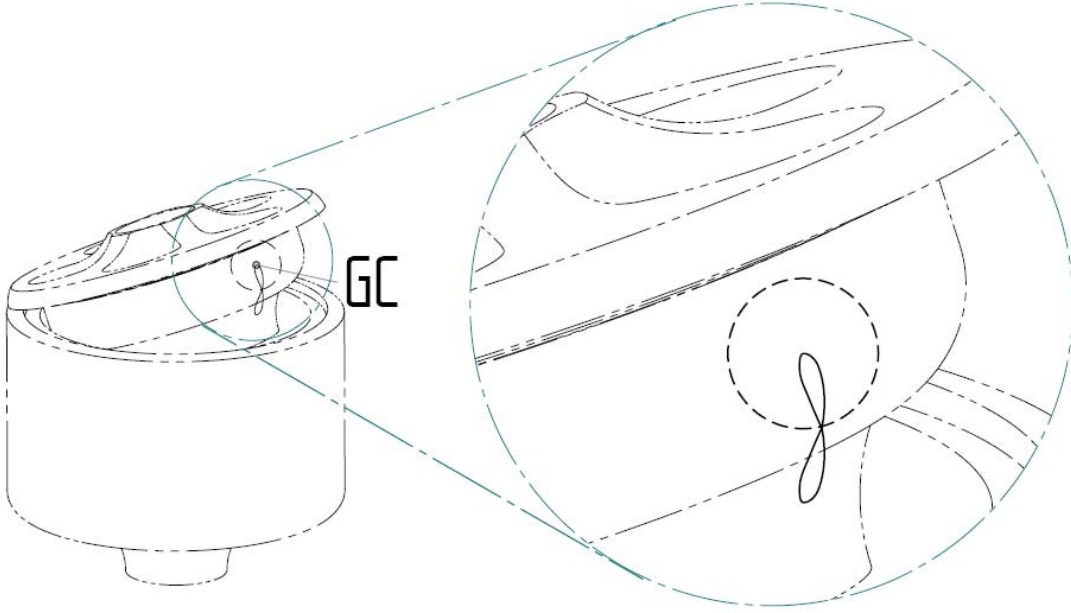


Figure 16 – The vector \bar{r}_{GC} forms a double closed loop. If placed in the nobble plane, the projection of the trajectory upon the ${}^N x^N y$ -plane forms a circle and the vertical displacement is purely sinusoidal as seen in Figure 17 and Eq. 5. Note that the dashed circle in this figure depicts GC.

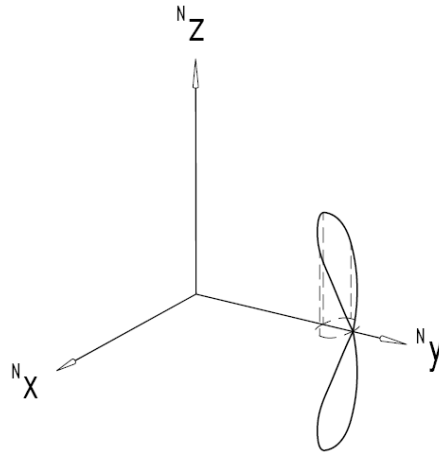


Figure 17 – The trajectory of \bar{r}_{GC} and the circular projection in the ${}^N x^N y$ -plane.

$${}^N[\bar{r}_{GC}] = [R_{W \rightarrow N}]^W[\bar{r}_{GC}] = \begin{bmatrix} \frac{1}{2} \sin(2 \cdot \varphi) \cdot (1 - \cos \alpha) \cdot R \\ \frac{1}{2} (1 + \cos \alpha + \cos(2 \cdot \varphi) \cdot (\cos \alpha - 1)) \cdot R \\ \cos \varphi \cdot \sin \alpha \cdot R \end{bmatrix} \quad \text{Eq. 5}$$

The diameter of the circular projection of the trajectory in Figure 17 is named D_{GC} and follows the expression in Eq. 6.

$$D_{GC} = \max(\bar{r}_{GC} \bullet \bar{e}_{N_y}) - \min(\bar{r}_{GC} \bullet \bar{e}_{N_y}) = R \cdot (1 - \cos \alpha) \quad \text{Eq. 6}$$

4.1.4 Piston

To determine the vector expression of the piston position (Eqs. 7 and 8) we define three vectors; \bar{r}_p pointing to the piston centre of mass with the radial position y_{cyl} (constant) and the vertical position z_{cyl} (variable), the position of the lower ball joint of the associated piston rod is described by the vector \bar{r}_{GC} (Figure 18) and a vector \bar{r}_H between the two points GC and P is defined (Figure 18). To solve for z_{cyl} , the length of the vector \bar{r}_H is set to l_{pr}

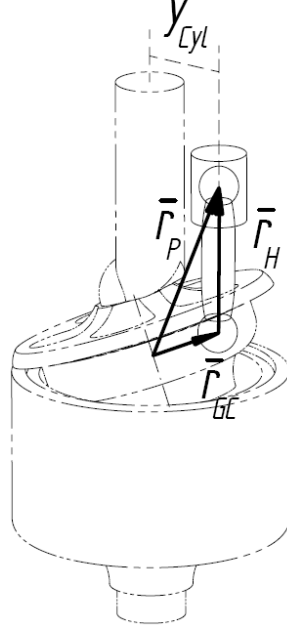


Figure 18 – Illustration of the involved vectors in deriving the piston vertical position, z_{cyl} . Vector \bar{r}_{GC} points to the lower ball joint of the piston rod. Vector \bar{r}_P points to the piston centre of mass. Vector \bar{r}_H is the vector between the two points GC and P.

$${}^N[\bar{r}_{P,1}] = {}^N \begin{bmatrix} 0 & y_{cyl} & z_{cyl} \end{bmatrix}$$

Eq. 7

$$\left\| {}^N[\bar{r}_{H,1}] \right\| = \left\| {}^N[\bar{r}_{P,1} - \bar{r}_{GC,1}] \right\| = l_{Pr} \Rightarrow z_{cyl} = f(\varphi, \alpha, R, y_{cyl}, l_{Pr})$$

If the piston is placed directly above the circular trajectory (Figure 17) formed by GC in the ${}^N\mathcal{X}^N y$ -plane, the vertical translation of the piston reduces to a pure sinusoidal motion.

$${}^N[\bar{r}_{P,1}] = {}^N \begin{bmatrix} 0 & y_{cyl} & z_{cyl} \end{bmatrix} \Rightarrow \left\{ y_{cyl} = \max(\bar{r}_{GC} \cdot \bar{e}_{N_y}) - \frac{1}{2} \cdot D_{CC} \right\} \Rightarrow$$

Eq. 8

$${}^N[\bar{r}_P] = {}^N \begin{bmatrix} 0 & \frac{1}{2} R \cdot (1 + \cos \alpha) & R \cdot \sin \alpha \cdot \cos \varphi + 2 \cdot l_{Pr} \cdot \cos \beta \end{bmatrix}$$

4.1.5 Piston rod

The two endpoints of the piston rod are known, \bar{r}_P and \bar{r}_{GC} , and it is now possible to derive the centre of mass vector of the piston rod. In order to simplify the centre of mass vector expression and further to simplify the derivation of the dynamics calculations (e.g. mass moment of inertia matrix) the body-fixed coordinate system of the piston rod is

sought for. Defining three coordinate systems (Pr1, Pr2 and Pr3) following the 1-3-1 convention of Euler angles (see Figure 14), a vector written in the body-fixed coordinate system pointing from GC to P can be defined. Solving for the unknown Euler angles, the variables describing the intermediate rotations of the coordinate systems are found (the third coordinate system is not depicted nor does its angle of rotation appear in the equations since two rotations are sufficient in finding the orientation of the piston rod).

In order to solve for γ and β explicitly, the vector \bar{r}_p is set to equal a second vector \bar{r}_{p_i} Eq. 9.

$$\bar{r}_{p,i} = \bar{r}_{GC,i} + {}^{\text{Pr}2,1} [0 \quad 0 \quad l_{\text{pr}}] \quad \text{Eq. 9}$$

The equality of \bar{r}_p and \bar{r}_{p_i} gives (after simplification) the expressions in Eq. 10.

$$\begin{aligned} \gamma &= 2 \cdot \varphi \\ \beta &= -\arcsin\left(\frac{D_{GC}/2}{l_{\text{pr}}}\right) \end{aligned} \quad \text{Eq. 10}$$

This concludes the kinematical modeling of the machine.

4.2 Dynamical model

The dynamical modelling of the machine is a matter of formulating the Euler equations of motion. The equations in themselves make no difference between forward dynamics (where known applied loads result in a dynamical motion of the system of bodies) or inverse dynamics (where a given motion of the system together with known applied loads gives requisite loads upon the system to satisfy the motion) though the model presented here will be of the latter type. The choice to present results from inverse dynamics simulations is done since the braking or driving torque upon the Z-shaft then doesn't have to be modelled. This also eliminates lengthy integration times associated with achieving steady-state conditions.

Mechanical joints between the integral parts of the machine are defined along the design concept in Figure 11. The constraints of the integral joints of the machine are applied to the bodies, as are the known applied loads (e.g., steam pressure and gravity), which, together with component mass and mass moment of inertia, form the Euler equations. A simplified model of the steam pressure as a function of the Z-shaft angle of rotation is then described, which acts on the system of bodies as a force applied to the pistons.

The inertias of the integral parts of the system of bodies determine if non-zero external loads are required to keep the machine from translating or rotating. If the inertias can be configured such that they cancel each other out, the machine is said to be balanced.

4.2.1 Inverse dynamics

The method of inverse dynamics is used when the motion (i.e., positions, orientation, velocities, and accelerations) of a system of rigid bodies is known; the method yields the required external and internal forces and torques (Figure 19) from the equations of motion. A rigid-body system is a collection of bodies that may be connected together by joints and that may be acted on by various loads [17]. Known loads are distinguished from constraint loads, the latter ensuring that the prescribed motion is completely determined by loads. The Euler equations of motion are Eqs. 11 and 12.

$$\bar{\mathbf{R}} + \bar{\mathbf{F}}_a = m \cdot \ddot{\mathbf{r}}_G \quad \text{Eq. 11}$$

$$\bar{\mathbf{T}} + \bar{\mathbf{M}}_a + \bar{\mathbf{r}}_R \times \bar{\mathbf{R}} + \bar{\mathbf{r}}_F \times \bar{\mathbf{F}}_a = \frac{d}{dt}(\mathbf{J}\dot{\boldsymbol{\phi}}) \quad \text{Eq. 12}$$

where $\bar{\mathbf{F}}_a$, $\bar{\mathbf{M}}_a$, $\bar{\mathbf{r}}_R$, $\bar{\mathbf{r}}_F$, $m \cdot \ddot{\mathbf{r}}_G$, and $\frac{d}{dt}(\mathbf{J}\dot{\boldsymbol{\phi}})$ are considered as known, and $\bar{\mathbf{R}}$ and $\bar{\mathbf{T}}$ as unknown constraint loads.

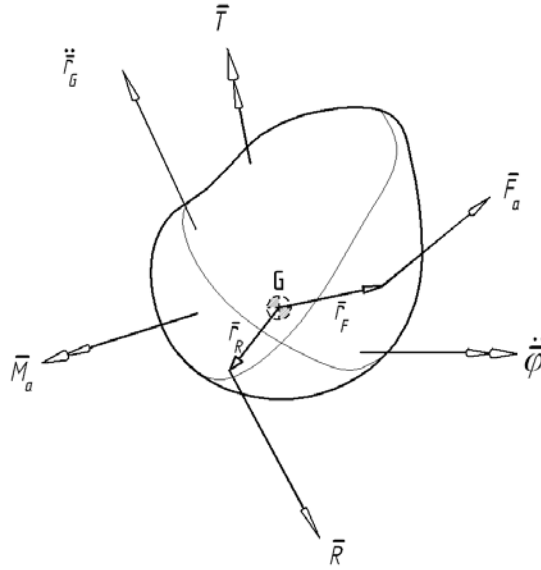


Figure 19 – The known and unknown force and torque vectors affecting the motion of a body with mass and mass moment of inertia.

The only variables are \bar{R} and \bar{T} , so the equations of motion form a system of linear algebraic equations. Such a system has a unique solution if the determinant of the matrix collecting the coefficients of the unknown is non-zero. One strength of an inverse dynamic model is its ability to provide results even when the motion of the system of bodies is not completely determined by the known applied loads.

4.2.2 Performance of mechanical work

Because of the separation between known and unknown loads, the constraint loads are able to perform mechanical work. The equations of motion are applicable for both forward and inverse simulations, and if the known applied loads are sufficient to result in the stipulated motion the constraint loads will not perform mechanical work. During steady-state conditions the net work performed upon the machine shall equal zero since the model models a loss-free mechanism neglecting friction or media losses and accumulated energy, Figure 20 and Eqs. 13, 14 and 15.

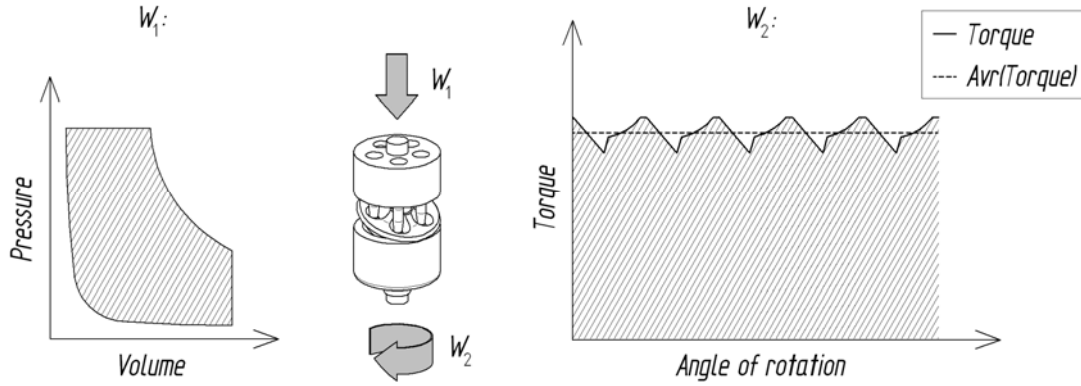


Figure 20 – The performance of mechanical work on the machine. The area of the cylinder indicator diagram (pressure–volume) multiplied by the number of cylinders, n_p , represents the input work, W_1 , over one shaft revolution. This work must be balanced by W_2 , i.e., the work absorbed by the brake torque applied to the Z-shaft, over one shaft revolution.

$$W_1 = \sum_{i=1}^{i=n_p} \oint p_i dV_i \quad \text{Eq. 13}$$

$$W_2 = \int_0^{2\pi} \bar{T}_{ZE} \cdot d\bar{\varphi} \quad \text{Eq. 14}$$

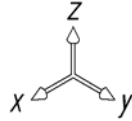
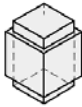



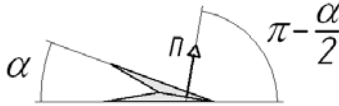

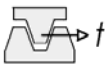
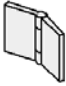
$$\text{Energy conservation: } W_1 = W_2 \quad \text{Eq. 15}$$

where p_i is the pressure inside cylinder i , V_i is the volume of cylinder i and \bar{T}_{ZE} is the engine shaft torque.

4.2.3 Integral mechanical joints

The design concept requires six types of joints that, when applied between bodies or from ground to body, will define the allowed and unallowed directions of motion. An unallowed or restricted direction of motion presupposes the loads necessary to prevent such relative motion between bodies or between body and ground. If a joint interconnects bodies, the defined loads on one of the bodies must be mirrored on the other, according to the law of reciprocal action. The occurring joints are presented in Table 2, where the allowed and restricted directions of motion are defined.

Table 2 – The integral joints of the dynamic model presented in this paper.

			Coordinate system
			
Joint type	Illustration	Constraining directions	Allowed directions of motion
Translational		Translation: x, y Rotation: x, y, z	Translation: z
Ball		Translation: x, y, z	Rotation: x, y, z
Cylindrical		Translation: x, y Rotation: x, y	Translation: z Rotation: z
Cone		Translation: n 	Translation: <i>orthogonal to n</i> Rotation: x, y, z
Gear		Translation: t 	Translation: <i>orthogonal to t</i> Rotation: x, y, z
Revolute		Translation: x, y, z Rotation: x, y	Rotation: z

4.2.4 Systems of bodies connected by joints

The joints in Table 2 are applied to the integral parts of the machine, which are depicted in Figure 21.

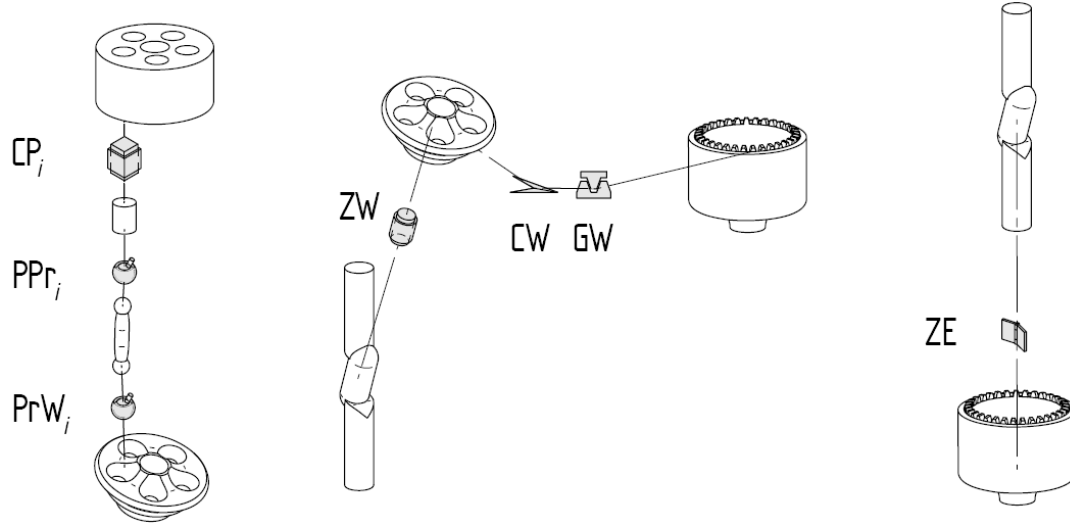


Figure 21 – The joints connecting the integral parts of the machine: translational joint CP_i connecting the cylinder head and piston number i , ball joint PPr_i connecting piston number i and piston rod number i , ball joint PrW_i connecting piston rod number i and the wobble plate, cylindrical joint ZW connecting the Z-shaft and wobble plate, cone joint CW connecting the wobble plate and engine block, gear joint GW connecting the wobble plate and engine block, and revolute joint ZE connecting the Z-shaft and engine block.

The connection scheme is compiled and presented in Table 3 (with added fixed joints).

Table 3 – A joint label in one cell indicates that the specified joint connects the body or ground to the body or ground specified in the labels of the row and column containing the cell. For example, cell (2,4) specifies that the two joints CW and GW connect the engine block to the wobble plate.

	Ground	Engine block	Z-shaft	Wobble plate	Piston rod	Piston	Cylinder head	Ground
Ground	1	Fixed						
Engine block	Fixed	1	ZE	CW, GW				
Z-shaft		ZE	1	ZW				
Wobble plate		CW, GW	ZW	1	PrW_i			
Piston rod				PrW_i	1	PP_{r_i}		
Piston					PP_{r_i}	1	CP_i	
Cylinder head						CP_i	1	Fixed
Ground							Fixed	1

The directions in which the joints are defined and the constraint loads are applied are presented in Table 4, where the first three components of the vector correspond to forces and translations and the last three to torques and rotations.

Table 4 – The coordinate systems in which the joints are defined, where a vector component of value 1 indicates applying a constraint load in this direction and a component of value q indicates that a constraint load is able to perform mechanical work if applied in this direction.

Joint name	Coordinate system
ZE	${}^N[\bar{t}_{ZE}] = [1 \quad 1 \quad 1 \quad 1 \quad 1 \quad q]$
ZW	${}^T[\bar{t}_{ZW}] = [1 \quad 1 \quad q \quad 1 \quad 1 \quad q]$
GW	${}^T[\bar{t}_{GW}] = [1 \quad q \quad q \quad q \quad q \quad q]$
CW	${}^K[\bar{t}_{CW}] = [q \quad q \quad 1 \quad q \quad q \quad q]$
PrW_i	${}^N[\bar{t}_{PrW,i}] = [1 \quad 1 \quad 1 \quad q \quad q \quad q]$
PPr_i	${}^N[\bar{t}_{PPr,i}] = [1 \quad 1 \quad 1 \quad q \quad q \quad q]$
CP_i	${}^N[\bar{t}_{CP,i}] = [1 \quad 1 \quad q \quad 1 \quad 1 \quad 1]$

4.2.5 System of equations

For each component (rigid body), the vector sums of unknown constraint loads (forces and torques) from the joints and from the known applied loads are set equal to the inertia terms defined by the components' kinematics, mass, and moment of inertia. For a machine with five cylinders, this forms a linear system of 72 algebraic equations and 66 unknown constraint loads. Five additional constraint loads have to be introduced for the torque components corresponding to the piston rods' rotational degree of freedom around their symmetry axes. One additional constraint load, the brake torque acting on the engine shaft, also has to be introduced. Thus, the number of unknowns becomes 72.

Piston:

$$\bar{R}_{CP,i} - \bar{R}_{PPr,i} + \bar{F}_{a,P,i} = m_P \cdot \ddot{\bar{r}}_{CM,P,i}$$

$$\bar{T}_{P,i} + \bar{M}_{a,P,i} + \bar{r}_{R_{CP,i}} \times \bar{R}_{CP,i} + \bar{r}_{R_{PPr,i}} \times (-\bar{R}_{PPr,i}) + \bar{r}_{F,P,i} \times \bar{F}_{a,P,i} = \frac{d}{dt} (J_{P,i} \dot{\bar{\phi}}_{P,i})$$

$$Unknowns : \bar{R}_{CP,i} \in^N \{x, y\}, \bar{R}_{PPr,i} \in^N \{x, y, z\}, \bar{T}_P \in^N \{x, y, z\}$$

Piston rod:

$$\bar{R}_{PPr,i} - \bar{R}_{PrW,i} + \bar{F}_{a,Pr,i} = m_{Pr} \cdot \ddot{\bar{r}}_{CM,Pr,i}$$

$$\bar{T}_{Pr,i} + \bar{M}_{a,Pr,i} + \bar{r}_{R_{PPr,i}} \times \bar{R}_{PPr,i} + \bar{r}_{R_{PrW,i}} \times (-\bar{R}_{PrW,i}) + \bar{r}_{F,Pr,i} \times \bar{F}_{a,Pr,i} = \frac{d}{dt} (J_{Pr,i} \dot{\bar{\phi}}_{Pr,i})$$

$$Unknowns : \bar{R}_{PrW,i} \in^N \{x, y, z\}, \bar{T}_{Pr} \in^{Pr2,i} \{z\}$$

Wobble plate:

$$\bar{R}_{ZW} + \sum_{i=1}^5 \bar{R}_{PrW,i} + \bar{R}_{CW} + \bar{R}_{GW} + \bar{F}_{a,W} = m_W \cdot \ddot{\bar{r}}_{CM,W}$$

$$\bar{T}_{ZW} + \bar{M}_{a,W} + \sum_{i=1}^5 (\bar{r}_{R_{PrW,i}} \times \bar{R}_{PrW,i}) + \bar{r}_{R_{ZW}} \times \bar{R}_{ZW} + \bar{r}_{R_{CW}} \times \bar{R}_{CW} + \bar{r}_{R_{GW}} \times \bar{R}_{GW} + \bar{r}_{F,W} \times \bar{F}_{a,W} = \frac{d}{dt} (J_W \dot{\bar{\phi}}_W)$$

$$Unknowns : \bar{R}_{ZW} \in^W \{x, y\}, \bar{R}_{CW} \in^K \{z\}, \bar{R}_{GW} \in^T \{x\}, \bar{T}_P \in^W \{x, y\}$$

Z-shaft:

$$\bar{R}_{ZE} - \bar{R}_{ZW} + \bar{F}_{a,Z} = m_Z \cdot \ddot{\bar{r}}_{CM,Z}$$

$$\bar{T}_{ZE} + \bar{M}_{a,Z} + \bar{r}_{R_{ZW}} \times (-\bar{R}_{ZW}) + \bar{r}_{R_{ZE}} \times \bar{R}_{ZE} + \bar{r}_{F,Z} \times \bar{F}_{a,Z} = \frac{d}{dt} (J_Z \dot{\bar{\phi}}_Z)$$

$$Unknowns : \bar{R}_{ZE} \in^N \{x, y, z\}, \bar{T}_{ZE} \in^N \{x, y, z\}$$

The above system of equations for solving the inverse dynamics, can be re-written in matrix form as follows in Eq. 16:

$$A \cdot \bar{x} = \bar{b} \tag{Eq. 16}$$

where matrix A is the coefficient matrix, vector \bar{x} comprises the unknown loads \bar{R} and \bar{T} and vector \bar{b} constitutes the constant terms of the equations.

This system of equations is linear. Such a system is solvable if $\det(A) \neq 0$, which is equivalent to a statically determined system (as opposed to an under- or over-constrained system).

4.3 Balancing of inertias

There is a possibility to completely balance the inertia loads of the machine by proper configuration of some geometrical parameters and by means of dead-weights. The analysis concerning balancing is hereby presented.

The moving parts of the machine are pistons, piston rods, wobble plate and Z-shaft. If not configured properly with respect to centre of mass placement and configuration of mass and mass moment of inertia matrix, the machine will require external loads to restrain it from vibrations (translations and rotations) due to the inertia of the moving parts. As will be showed the inertias can be balanced by two means, either by self balancing by symmetry and selection of proper geometric parameters or by dead-weights upon the Z-shaft. An example of the first balancing principle is the self balancing achieved by the piston rods motions if the piston is placed at the radial position y_{Cyl} , the change in momentum and angular momentum in the $^N\mathcal{X}^N\mathcal{Y}$ -plane will equal zero and no external lateral forces or torques are required to keep the machine in place. An example of the latter is balancing out the inertias from the wobble plate's nutating motion by means of dead-weights upon the Z-shaft. The self balancing by symmetry presupposes that the pistons and piston rods respectively are of the same mass and placed symmetrical around the Z-shaft. The general equations governing balancing of inertias follow Eqs. 17 and 18.

$$\sum_k m_i \cdot \ddot{\vec{r}}_i + \sum_m m_j \cdot \ddot{\vec{r}}_j = 0 \quad \text{Eq. 17}$$

$$\sum_k \left(\vec{r}_{CM,i} \times (m_i \cdot \ddot{\vec{r}}_{CM,i}) + \frac{d}{dt} (J_i \dot{\vec{\varphi}}_i) \right) + \sum_m \left(\vec{r}_{CM,j} \times (m_j \cdot \ddot{\vec{r}}_{CM,j}) + \frac{d}{dt} (J_j \dot{\vec{\varphi}}_j) \right) = 0 \quad \text{Eq. 18}$$

4.3.1 Pistons

If the pistons are placed directly above the circle centre of the projection of \vec{r}_{GC} in the $^N\mathcal{X}^N\mathcal{Y}$ -plane, their motions will be pure sinusoidal. The net inertia load from the translation of the pistons is stated in Eqs. 19 and 20.

$$\vec{F}_P = \sum_{i=1}^n (\vec{F}_{P,i}) = \sum_{i=1}^n (m_{P,i} \cdot \ddot{\vec{r}}_{CM,P,i}) \quad \text{Eq. 19}$$

$$\bar{M}_P = \sum_{i=1}^n (\bar{M}_{P,i}) = \sum_{i=1}^n \left(\frac{d}{dt} (J_{P,i} \dot{\bar{\varphi}}_{P,i}) + \bar{r}_{CM,P,i} \times \bar{F}_{P,i} \right) \quad \text{Eq. 20}$$

Since the only motion the pistons experience is translation about the space fixed vertical (${}^N \ddot{\bar{r}}_{CM,P,i} = {}^N [0 \quad 0 \quad f(\varphi, \dot{\varphi}, \ddot{\varphi}, R, \alpha,)]$ and $\dot{\bar{\varphi}}_{P,i} = \bar{0}$), the inertia load reduces to Eqs. 19' and 20'.

$${}^N [\bar{F}_{P,i}] = {}^N [0 \quad 0 \quad F_{P,i_z}] \quad \text{Eq. 19'}$$

$$\bar{M}_P = \sum_{i=1}^n (\bar{r}_{CM,P,i} \times \bar{F}_{P,i}) = \sum_{i=1}^n ({}^N [r_{CM,P,i_x} \cdot F_{P,i_z} \quad r_{CM,P,i_y} \cdot F_{P,i_z} \quad 0]) = \quad \text{Eq. 20'}$$

$$= \sum_{i=1}^n \left(-m_i y_{Cyl} R \sin \alpha \begin{bmatrix} \cos\left((i-1)\frac{2\pi}{n}\right) \left(\dot{\varphi}^2 \cos\left(\varphi - (i-1)\frac{2\pi}{n}\right) + \ddot{\varphi} \sin\left(\varphi - (i-1)\frac{2\pi}{n}\right) \right) \\ \sin\left((i-1)\frac{2\pi}{n}\right) \left(\dot{\varphi}^2 \cos\left(\varphi - (i-1)\frac{2\pi}{n}\right) + \ddot{\varphi} \sin\left(\varphi - (i-1)\frac{2\pi}{n}\right) \right) \\ 0 \end{bmatrix}^T \right) =$$

$$= \left\{ \begin{array}{l} \sum_{i=1}^n \cos\left((i-1)\frac{2\pi}{n}\right) \cos\left(\varphi - (i-1)\frac{2\pi}{n}\right) = \frac{n}{2} \cos(\varphi) \\ \sum_{i=1}^n \cos\left((i-1)\frac{2\pi}{n}\right) \sin\left(\varphi - (i-1)\frac{2\pi}{n}\right) = \frac{n}{2} \sin(\varphi) \\ \sum_{i=1}^n \sin\left((i-1)\frac{2\pi}{n}\right) \cos\left(\varphi - (i-1)\frac{2\pi}{n}\right) = \frac{n}{2} \sin(\varphi) \\ \sum_{i=1}^n \sin\left((i-1)\frac{2\pi}{n}\right) \sin\left(\varphi - (i-1)\frac{2\pi}{n}\right) = -\frac{n}{2} \cos(\varphi) \end{array} \right\} =$$

$$= -m_P \frac{n}{2} y_{Cyl} R \sin \alpha \begin{bmatrix} \dot{\varphi}^2 \cdot \cos \varphi + \ddot{\varphi} \cdot \sin \varphi \\ \dot{\varphi}^2 \cdot \sin \varphi - \ddot{\varphi} \cdot \cos \varphi \\ 0 \end{bmatrix}^T, \quad \text{for } n \geq 2$$

The only inertia loads from the pistons are thus lateral torques, and counter balancing lateral torques can be achieved by implementing cross-terms in the Z-shaft inertia matrix. An inertia matrix of the Z-shaft is formulated, including the cross-terms $J_{Z,BP_{xz}}$ and

$J_{Z,BP_{yz}}$. The sum of the change in angular momentum of the Z-shaft and the inertia torque of the pistons are set to equal zero. This equation can be solved for the cross-terms and the resulting formulas indicate the mass moment of inertia necessary to counter-balance the inertia load of the pistons Eq 21.

$$\frac{d}{dt} \left(\begin{bmatrix} J_{Z_{xx}} & 0 & J_{Z,BP_{xz}} \\ 0 & J_{Z_{yy}} & J_{Z,BP_{yz}} \\ J_{Z,BP_{xz}} & J_{Z,BP_{yz}} & J_{Z_{zz}} \end{bmatrix} \cdot \dot{\vec{\phi}}_Z \right) + \sum_{i=1}^n (\overline{M}_{P,i}) = \overline{0} \quad \text{Eq. 21}$$

Eq. X is solved for the cross-terms $J_{Z,BP_{xz}}$ and $J_{Z,BP_{yz}}$, which gives Eq. 22.

$$J_{Z,BP_{yz}} = 0, \quad J_{Z,BP_{xz}} = -m_p \frac{n}{2} y_{Cyl} R \sin \alpha, \quad \text{for } n \geq 3 \quad \text{Eq. 22}$$

To summarize, given that the pistons are of same mass, and with centre of mass placed at the centre of the ball joint connecting piston and piston rod; placing GC_i in the wobble plane and the radial position of the pistons to y_{Cyl} will result in sinusoidal motion of the pistons. The vertical acceleration of the pistons results in an inertia torque, but no inertia force. The inertia torque is out-balanced by dead-weights upon the Z-shaft, i.e. cross-terms in the inertia matrix of the Z-shaft, see Eq. 22. The number of pistons has to be 3 or higher.

4.3.2 Piston rods

The same principle as to counter-balancing the inertia loads of the pistons is applied to the piston rods, i.e. counter-balancing the inertia load from the vertical and lateral accelerations of the centres of mass of the piston rods by cross-terms in the Z-shaft inertia matrix, Eq. 23. The centre of mass is at a variable distance from the $^N\hat{x}$ -axis (the piston rods centres of mass follow a double-closed loop).

$$\frac{d}{dt} \left(\begin{bmatrix} J_{Z_{xx}} & 0 & J_{Z,BPr_{xz}} \\ 0 & J_{Z_{yy}} & J_{Z,BPr_{yz}} \\ J_{Z,BPr_{xz}} & J_{Z,BPr_{yz}} & J_{Z_{zz}} \end{bmatrix} \cdot \dot{\vec{\phi}}_Z \right) + \sum_{i=1}^n (\overline{M}_{Pr,i}) = \overline{0} \quad \text{Eq. 23}$$

$$\text{Where } \overline{M}_{Pr} = \sum_{i=1}^n (\vec{r}_{CM,Pr,i} \times \vec{F}_{Pr,i}) = \sum_{i=1}^n (\vec{r}_{CM,Pr,i} \times (m_{Pr,i} \cdot \ddot{\vec{r}}_{CM,Pr,i}))$$

The positions of the centres of mass are written on simplified form as follows, Eq. 24.

$$\begin{aligned} \bar{r}_{CM,Pr,i} &= \bar{r}_{GC,i} + {}^{Pr}2,i \begin{bmatrix} 0 & 0 & l_{Pr} / 2 \end{bmatrix} = \\ &= \begin{bmatrix} -y_{Cyl} \cdot \sin\left(\frac{(i-1) \cdot 2\pi}{n}\right) - C_{Pr} \cdot \sin\left(2 \cdot \varphi - \frac{(i-1) \cdot 2\pi}{n}\right) \\ y_{Cyl} \cdot \cos\left(\frac{(i-1) \cdot 2\pi}{n}\right) + C_{Pr} \cdot \cos\left(2 \cdot \varphi - \frac{(i-1) \cdot 2\pi}{n}\right) \\ \cos\left(-\frac{(i-1) \cdot 2\pi}{n} + \varphi\right) \cdot \sin \alpha \cdot R + \frac{l_{Pr}}{2} \cdot \cos \beta \end{bmatrix} \end{aligned} \quad \text{Eq. 24}$$

And the acceleration thus becomes, Eq. 25:

$$\ddot{\bar{r}}_{CM,Pr,i} = \begin{bmatrix} C_{Pr} \cdot \left(4 \cdot \sin\left(-\frac{(i-1) \cdot 2\pi}{n} + 2\varphi\right) \cdot \dot{\varphi}^2 - 2 \cdot \cos\left(-\frac{(i-1) \cdot 2\pi}{n} + 2\varphi\right) \cdot \ddot{\varphi} \right) \\ C_{Pr} \cdot \left(-4 \cdot \cos\left(-\frac{(i-1) \cdot 2\pi}{n} + 2\varphi\right) \cdot \dot{\varphi}^2 - 2 \cdot \sin\left(-\frac{(i-1) \cdot 2\pi}{n} + 2\varphi\right) \cdot \ddot{\varphi} \right) \\ -C_1 \cdot \left(\cos\left(-\frac{(i-1) \cdot 2\pi}{n} + \varphi\right) \cdot \dot{\varphi}^2 + \sin\left(-\frac{(i-1) \cdot 2\pi}{n} + \varphi\right) \cdot \ddot{\varphi} \right) \end{bmatrix} \quad \text{Eq. 25}$$

Where $C_{Pr} = \frac{l_{Pr}}{2} \cdot \sin \beta$ and $C_1 = R \cdot \sin \alpha$

Therefore, the torque becomes, Eq. 26:

$$\begin{aligned}
\bar{M}_{\text{Pr}} &= \sum_{i=1}^n (\bar{r}_{CM, \text{Pr}, i} \times (m_{\text{Pr}, i} \cdot \ddot{\bar{r}}_{CM, \text{Pr}, i})) = \\
&= -m_{\text{Pr}} \cdot C_{\text{Pr}} \cdot \sum_{i=1}^N \left(\begin{array}{c} \cos\left(-\frac{(k-1) \cdot 2\pi}{n} + \varphi\right) \cdot C_1 + \\ + \frac{l_{\text{Pr}}}{2} \cdot \cos \beta \end{array} \right) \cdot \left[\begin{array}{c} \left(\begin{array}{c} -4\dot{\varphi}^2 \cos\left(-\frac{(k-1) \cdot 2\pi}{n} + 2\varphi\right) + \\ -2\ddot{\varphi} \sin\left(-\frac{(k-1) \cdot 2\pi}{n} + 2\varphi\right) \end{array} \right) \\ \left(\begin{array}{c} 4\dot{\varphi}^2 \sin\left(-\frac{(k-1) \cdot 2\pi}{n} + 2\varphi\right) + \\ -2\ddot{\varphi} \cos\left(-\frac{(k-1) \cdot 2\pi}{n} + 2\varphi\right) \end{array} \right) \\ 0 \end{array} \right] + \\
&+ m_{\text{Pr}} \cdot C_1 \cdot \sum_{i=1}^N \left(\begin{array}{c} \dot{\varphi}^2 \cos\left(-\frac{(k-1) \cdot 2\pi}{n} + \varphi\right) + \\ -\ddot{\varphi} \sin\left(-\frac{(k-1) \cdot 2\pi}{n} + \varphi\right) \end{array} \right) \cdot \left[\begin{array}{c} - \left(\begin{array}{c} y_{\text{Cyl}} \cdot \cos\left(\frac{(k-1) \cdot 2\pi}{n}\right) + \\ + C_{\text{Pr}} \cdot \cos\left(-\frac{(k-1) \cdot 2\pi}{n} + 2\varphi\right) \end{array} \right) \\ \left(\begin{array}{c} y_{\text{Cyl}} \cdot \sin\left(\frac{(k-1) \cdot 2\pi}{n}\right) + \\ + C_{\text{Pr}} \cdot \sin\left(-\frac{(k-1) \cdot 2\pi}{n} + 2\varphi\right) \end{array} \right) \\ 0 \end{array} \right] \\
\Rightarrow \bar{M}_{\text{Pr}} = \frac{1}{2} \cdot n \cdot m_{\text{Pr}} \cdot \left[\begin{array}{c} -C_1 \cdot y_{\text{Cyl}} - C_1 \cdot C_{\text{Pr}} + 4 \cdot \sin \alpha \cdot R \cdot C_{\text{Pr}} \\ C_1 \cdot y_{\text{Cyl}} - C_1 \cdot C_{\text{Pr}} - 2 \cdot \sin \alpha \cdot R \cdot C_{\text{Pr}} \\ 0 \end{array} \right] \quad \text{Eq. 26}
\end{aligned}$$

And solving Eq. 23 thus gives, Eq. 27:

$$J_{Z, B \text{Pr}_{xz}} = 0, \quad J_{Z, B \text{Pr}_{xy}} = \frac{1}{2} \cdot n \cdot m_{\text{Pr}} \cdot (-C_1 \cdot y_{\text{Cyl}} - C_1 \cdot C_{\text{Pr}} + 4 \cdot \sin \alpha \cdot R \cdot C_{\text{Pr}}) \quad \text{Eq. 27}$$

Now, since the piston rods centres of mass accelerate in the ${}^N\mathbf{x}^N\mathbf{y}$ -plane, they could give a net inertia force load in this direction as well. The same is true for the angular acceleration of the piston rods. It will now be shown that these will all reduce to zero given that the number of piston rods are two or more, the centre of mass of the piston rods are along the \hat{z} -axis of the coordinate systems Pr2,i, of the same mass and if the inertia matrix of the piston rods are diagonal.

The centres of mass of the piston rods follow the same trajectory as $\bar{\mathbf{r}}_{GC}$ but with a different diameter unless at $\bar{\mathbf{r}}_{GC}$. The projection of the trajectory in the ${}^N\mathbf{x}^N\mathbf{y}$ -plane forms a circle and each piston rod centre of mass complete two laps along this circle over one Z-shaft revolution. Each centre of mass is phase-shifted $(i-1)\frac{2\pi}{n}$ at all times (Figure 22).

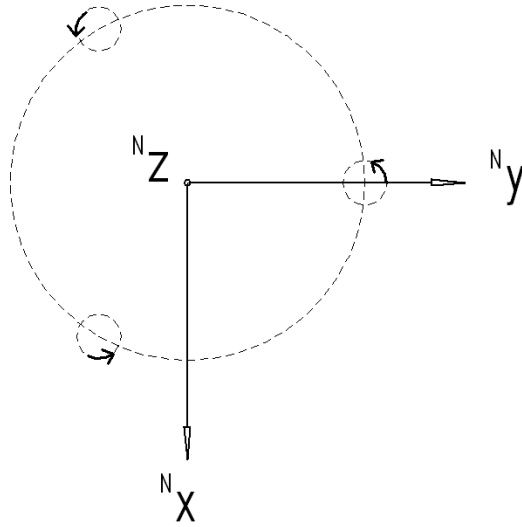


Figure 22 – An illustration of three piston rod centres of mass projected in the ${}^N\mathbf{x}^N\mathbf{y}$ -plane.

As illustrated in Figure 22 each piston rod centre of mass forms a circular trajectory with the circles centres being at a constant radius. After simplification, the accelerations reduce to Eq. 28. Thus, if the piston rods are of the same mass, the accelerations of the piston rods centres of mass counteract each other and therefore out-balance each other.

$$\sum_{i=1}^n \ddot{r}_{CM,Pr,i} = C_{Pr} \sum_{i=1}^n \begin{bmatrix} 4 \sin\left(2 \cdot \varphi - (i-1) \cdot \frac{2\pi}{n}\right) \cdot \dot{\varphi}^2 - 2 \cos\left(2 \cdot \varphi - (i-1) \cdot \frac{2\pi}{n}\right) \cdot \ddot{\varphi} \\ -4 \cos\left(2 \cdot \varphi - (i-1) \cdot \frac{2\pi}{n}\right) \cdot \dot{\varphi}^2 - 2 \sin\left(2 \cdot \varphi - (i-1) \cdot \frac{2\pi}{n}\right) \cdot \ddot{\varphi} \\ f(\varphi, \dot{\varphi}, \ddot{\varphi}, R, \alpha) \end{bmatrix}$$

$$= \begin{bmatrix} 0 \\ 0 \\ f(\varphi, \dot{\varphi}, \ddot{\varphi}, R, \alpha) \end{bmatrix} \text{ for } n \geq 2$$

Eq. 28

The same relation applies to the balancing of the lateral mass moment of inertias of the piston rods. All piston rods experience the angular acceleration $2\ddot{\varphi}$ around the $^N\hat{x}$ -axis, and are at a constant pitch β . Given that each piston rod is assigned an identical inertia matrix in their body-fixed coordinate system respectively and that they are symmetrical ($J_{Pr,i,xx} = J_{Pr,i,yy}$), balancing is achieved. The changes in angular momentum of the piston rods follow Eq. 29.

Eq. 29

$$\dot{\vec{L}}_{Pr,i} = \frac{d}{dt} \left(J_{Pr,i} \bullet \dot{\vec{\theta}}_i \right) =$$

$$= -\sin(2\beta) \cdot (-J_{Pr,i,zz} + J_{Pr,i,xx}) \begin{bmatrix} \sin\left(2 \cdot \varphi - (i-1) \cdot \frac{2\pi}{n}\right) \cdot \ddot{\varphi} + 2 \cos\left(2 \cdot \varphi - (i-1) \cdot \frac{2\pi}{n}\right) \cdot \dot{\varphi}^2 \\ -\cos\left(2 \cdot \varphi - (i-1) \cdot \frac{2\pi}{n}\right) \cdot \ddot{\varphi} + 2 \sin\left(2 \cdot \varphi - (i-1) \cdot \frac{2\pi}{n}\right) \cdot \dot{\varphi}^2 \\ f(\ddot{\varphi}, J_{Pr,i,xx}, J_{Pr,i,zz}, \beta) \end{bmatrix}$$

$$\Rightarrow \sum_{i=1}^n \dot{\vec{L}}_{Pr,i} = \begin{bmatrix} 0 \\ 0 \\ f(\ddot{\varphi}, J_{Pr,i..n,xx}, J_{Pr,i..n,zz}, \beta, n) \end{bmatrix}$$

Thus, the lateral inertia load from the change in mass moment of inertia of the piston rods is zero.

To summarize, given that the piston rods are of same mass, with centre of mass placed along the line of symmetry, and with symmetrical inertia matrix about the line of symmetry; placing GC_i in the wobble plane and the radial position of the pistons to J_{Cyl} will result in sinusoidal vertical motion and a completely circular lateral motion of the piston rods. The lateral acceleration of the piston rods will result in no inertia force or inertia torque. The vertical acceleration of the piston rods results in an inertia torque, but no inertia force. The inertia torque is out-balanced by dead-weights upon the Z-shaft, i.e. cross-terms in the inertia matrix of the Z-shaft, see Eq. 27. The number of piston rods has to be 2 or more to out-balance by symmetry and be 3 or higher to out-balance the inertia torque from the vertical acceleration of the piston rods.

4.3.3 Wobble plate

The out-balancing of the wobble plate is a matter of out-balancing the change in mass moment of inertia if the wobble plate centre of mass is placed at the (virtual) apexes of the cones since then the centre of mass does not move. This does only apply if the wobble plate is symmetrical, i.e. $J_{W_{xx}} = J_{W_{yy}}$. Two cross term counter-weight mass moment of inertia are defined in the Z-shaft inertia matrix, $J_{Z,BW_{xz}}$ and $J_{Z,BW_{yz}}$. The general Eq.8 applied to the sum of the Z-shaft and wobble plate change in angular momentum, Eq. 30.

Eq. 30

$$\begin{aligned}
\dot{\vec{L}}_W + \dot{\vec{L}}_Z &= 0 \Leftrightarrow \frac{d}{dt} \left(J_W \bullet \dot{\vec{\theta}}_W \right) + \frac{d}{dt} \left(J_Z \bullet \dot{\vec{\theta}}_Z \right) = \\
&= \frac{d}{dt} \left(\begin{bmatrix} J_{W_{xx}} & 0 & 0 \\ 0 & J_{W_{xx}} & 0 \\ 0 & 0 & J_{W_{zz}} \end{bmatrix} \bullet \dot{\vec{\theta}}_W \right) + \frac{d}{dt} \left(\begin{bmatrix} J_{Z_{xx}} & 0 & J_{Z,BW_{xz}} \\ J_{Z,BW_{xz}} & J_{W_{xx}} & J_{Z,BW_{yz}} \\ 0 & J_{Z,BW_{xz}} & J_{W_{zz}} \end{bmatrix} \bullet \dot{\vec{\theta}}_Z \right) = \\
&= \left[\begin{array}{l} -\sin \alpha \cdot \dot{\phi}^2 \cdot (-J_{W_{zz}} \cos \alpha + J_{W_{xx}} \cos \alpha + J_{W_{zz}}) - \dot{\phi}^2 \cdot J_{Z,BW_{yz}} \\ \sin \alpha \cdot \ddot{\phi} \cdot (-J_{W_{zz}} \cos \alpha + J_{W_{xx}} \cos \alpha + J_{W_{zz}}) + \ddot{\phi} \cdot J_{Z,BW_{yz}} \\ f(\ddot{\phi}, J_{W_{xx}}, J_{W_{zz}}, J_{Z_{zz}}, \alpha) \end{array} \right] = 0 \Rightarrow \\
\Rightarrow J_{Z,BW_{xz}} &= 0, \quad J_{Z,BW_{yz}} = -\sin \alpha \cdot (J_{W_{zz}} - J_{W_{xx}} \cos \alpha + J_{W_{xx}} \cos \alpha)
\end{aligned}$$

To summarize, given that the centre of mass of the wobble plate is placed in the apexes of the cones and that the inertia matrix is symmetrical about the wobble plate line of symmetry; the inertia of the wobble plate will result in an inertia torque but no inertia

force. The inertia torque is out-balanced by dead-weights upon the Z-shaft, i.e. cross-terms in the inertia matrix of the Z-shaft.

4.4 Cone-to-cone contact

An optimization routine would aid in the design process and could for example help in finding an optimal cone-to-cone radius R_{CW} for different material and bearing combinations. In the absence of an optimization routine applied to the mechanical model, the relation between cone-to-cone surface pressure and torque upon the Z-shaft is hereby explained. As shown in Paper C, the torque from the wobble plate upon the Z-shaft increases with increased radius R_{CW} . The contact force between wobble plate and engine block \bar{R}_{CW} is independent of the radius R_{CW} . The surface pressure at the contact line or contact point (if the surface is crowned in the direction parallel to the contact line) is proportional to the two radii's illustrated in Figure 23 and formulated in Eq. 31.

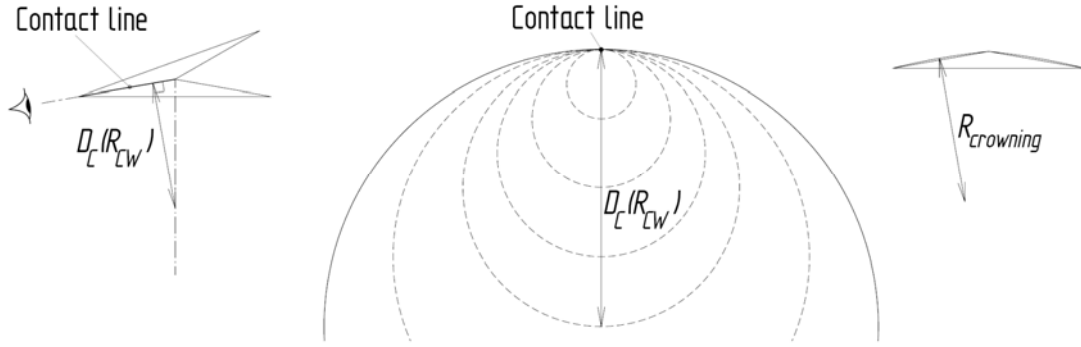


Figure 23 – An illustration of the two radii's defining the contact surface. A contact line is formed by the cone-to-cone contact. The curvature perpendicular to the contact line is illustrated in the middle image. The curvature parallel to the contact line is illustrated in the rightmost image.

$$D_c(R_{CW}) = \frac{R_{CW}}{\tan \frac{\alpha}{2}} \quad \text{Eq. 31}$$

Therefore, reducing the contact radius R_{CW} decreases the torque from the wobble plate upon the Z-shaft but increases the surface pressure in the cone-to-cone contact.

4.5 Cylinder pressure

The steam expansion and recompression in the cylinders have been approximated by isentropic (adiabatic loss-free) expansion and compression, thus roughly modelling the expansion (and recompression) parts of the thermodynamic Rankine cycle (see Figure 24). In reality, the pressure function will be smoother, especially at high speed, due to local throttling in valves and ports.

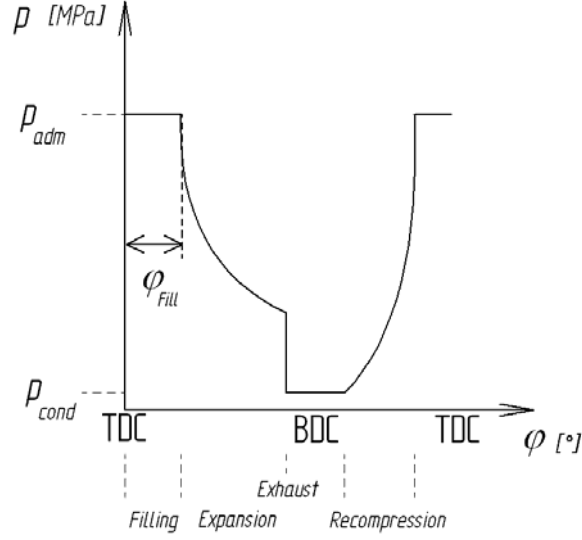


Figure 24 – A schematic of the approximating cylinder pressure function applied to the model as forces applied to the pistons.

The governing equation describing the expansion and compression will then be as follows in Eq. 32:

$$p_{isentropic}(\varphi) = p_0 \cdot \left(\frac{V(p_0)}{V(\varphi)} \right)^\kappa \quad \text{Eq. 32}$$

where φ is the shaft angle, p_0 the initial pressure at expansion/compression, $V(p_0)$ the initial volume at expansion/compression, $V(\varphi)$ the actual volume during expansion/compression, and κ the isentropic exponent.

The applied gas force on the pistons, $\bar{F}_{CP,a,i}$, is given by this pressure function multiplied by the area of the pistons, and phase shifted for each piston by $\frac{2\pi}{n_p}$, where n_p is the number of pistons.

4.6 Computing numerical results

To compute numerical results and generate graphs, input values for four different sets of parameters are required: mass and moment of inertia parameters, shaft rotation parameters, primary geometry parameters (e.g., piston rod length) and cylinder pressure parameters, see Table 5. These primary geometries are depicted in Figure 25.

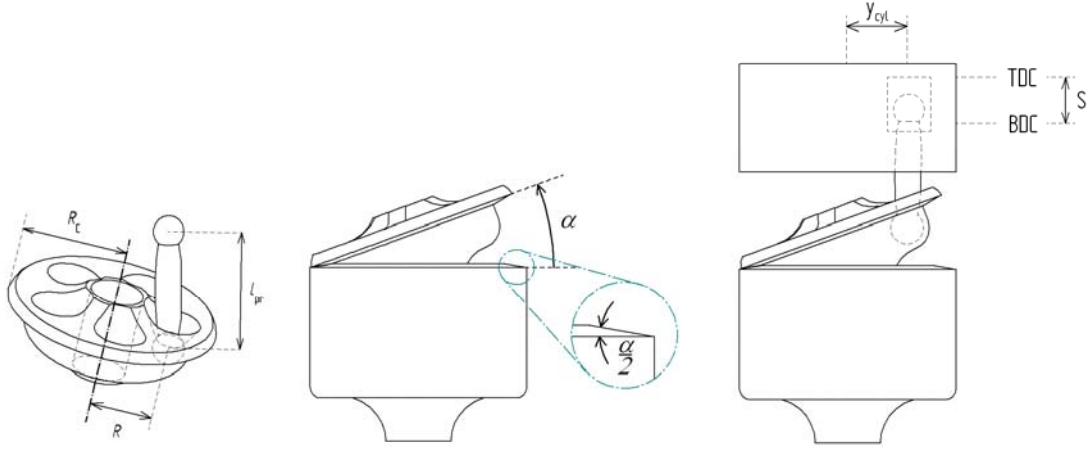


Figure 25 – The primary geometries $R_C = R_{CW}$, R , l_p , α , y_{cyl} and S .

Table 5 – The “default” values used to generate the results presented in the chapter “Results”.

Parameter class	Default parameter values
Mass and moment of inertia	All masses and mass moments of inertias equal zero.
Engine shaft rotation	$\varphi(t) = \omega \cdot t$, $\dot{\varphi}(t) = \omega$, $\ddot{\varphi}(t) = 0$ where $\omega = \frac{6000}{60} \cdot 2\pi \text{ rad/s}$
Geometry	$l_{Pr} = 0.2m$, $\alpha = 12.84^\circ$, $S = 0.04m$, $R = 0.09m$, $R_C = 0.1315m$, $A_p = \pi \cdot 0.02^2 m^2$ $\bar{r}_{R_{CP,i}} = \bar{0}$, $\bar{r}_{R_{Pr,i}} = {}^{Pr}2,i \begin{bmatrix} 0 & 0 & l_{Pr}/2 \end{bmatrix}$, $\bar{r}_{F,P,i} = \bar{0}$, $\bar{r}_{R_{PrW,i}} = {}^{Pr}2,i \begin{bmatrix} 0 & 0 & -l_{Pr}/2 \end{bmatrix}$, $\bar{r}_{F,Pr,i} = \bar{0}$, $\bar{r}_{R_{WPr,i}} = \begin{bmatrix} \cos\left(i \cdot \frac{2\pi}{5}\right) & \cos\left(i \cdot \frac{2\pi}{5}\right) & 0 \end{bmatrix} \cdot R$, $\bar{r}_{R_{ZW}} = \bar{0}$, $\bar{r}_{F,W} = \bar{0}$, $\bar{r}_{R_{ZE}} = \bar{0}$, $\bar{r}_{F,Z} = \bar{0}$, $n_p = 5$, $i = 1 \dots 5$
Cylinder pressure	$p_{adm} = 250 \cdot 10^5 Pa$, $p_{cond} = 1 \cdot 10^5 Pa$, $\kappa = 1.3$, $\varphi_{fill} = 90^\circ$

5 Results

Part of the results on contact loads and relative velocities presented in this thesis was used to construct a physical demonstrator of the machine, described in Chapter 4 Model and [16]. The results are presented in Figure 25, Table 6 and Table 7. The values in Figure 25 and Table 6 are computed for zero rotational velocity and zero gravitational acceleration. The values in Table 7 are computed for maximum rotational velocity 6000 rpm.

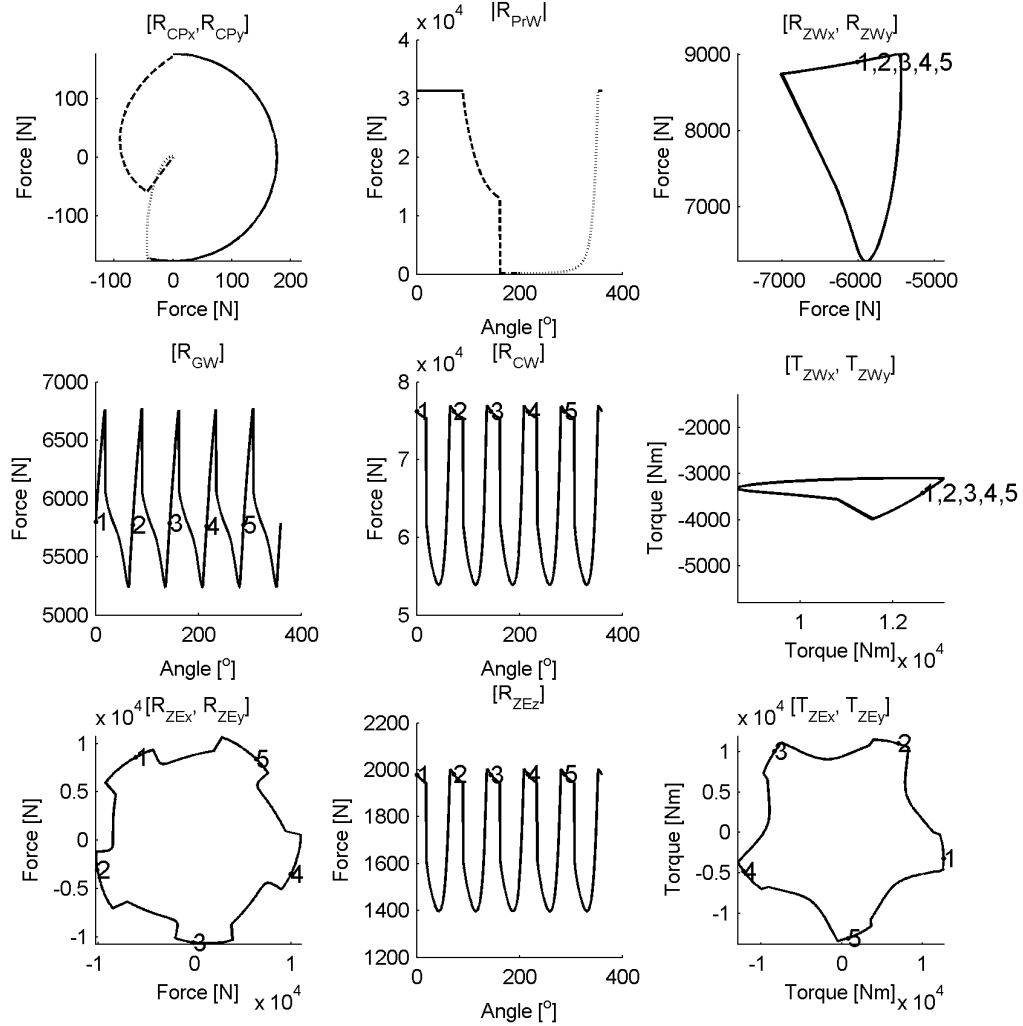


Figure 26 – The resulting loads in the joints with admission pressure 250 bar, cut-off 90° and mass-less integral parts. From left to right, from top to bottom (cells 1-9). The plot style of cell 1-2 indicate different states of steam pressure; solid line equals full admission pressure, dashed line equals expansion, dashed-dotted line equals open exhaust ports, dotted line equals compression. The numbers 1-5 in cells 3-9 indicates the opening of inlet valve for cylinder 1-5. 1. CP1: Lateral force in the contact between piston and cylinder liner. 2. PrW1: Force between piston rod and wobble plate. 3. ZW: Lateral force between wobble plate and Z-shaft. 4. GW: Tangential or gear force between wobble plate and engine block. 5. CW: Force in the cone contact between wobble plate and engine block. 6. ZW: Lateral torque between

wobble plate and Z-shaft. 7. ZE: Lateral force between Z-shaft and engine block. 8. ZE. Axial or vertical force between Z-shaft and engine block. 9. ZE. Lateral torque between Z-shaft and engine block.

The maximum absolute values of the contact loads in Figure 26 are summarized in Table 6.

Table 6 – Rounded values of the maximum load for the joints in Figure 26.

Contact	Maximum load
1. CP_i	176.7 N
2. PrW_i	31420 N
3. ZW	11220 N
4. GW	6773 N
5. CW	76990 N
6. ZW	13470 Nm
7. ZE	11050 N
8. ZE	2005 N
9. ZE	13460 Nm

The expressions and the maximum value for $n = 6000$ rpm of the relative velocity at these six contacts (CP_i , PrW_i , ZW , GW , CW , ZE) are summarized in Table 7..

Table 7 – Relative velocities in the six contacts ($CP1$, $PrW1$, ZW , GW , CW and ZE).

Contact	Expression	Relative velocity for $n = 6000$ rpm
CP_1	$\bar{v}_{CP,1} = \begin{bmatrix} 0 \\ 0 \\ -R_{GC} \cdot \sin \alpha \cdot \dot{\varphi} \cdot \sin \varphi \end{bmatrix}$	12.6 m/s
PrW_1	$\bar{v}_{PrW,1} = R_{PrW} \begin{bmatrix} \dot{\varphi} \cdot \sin \alpha \cos \varphi \\ \dot{\varphi} \cdot \sin \alpha \sin \varphi \\ 0 \end{bmatrix}$	2.1 m/s
ZW	$\bar{v}_{ZW} = \dot{\varphi}$	$\frac{6000}{60} \cdot 2\pi$ rad/s
GW	0	0
CW	0	0
ZE	$\bar{v}_{ZE} = \dot{\varphi}$	$\frac{6000}{60} \cdot 2\pi$ rad/s

Where R_{PrW} is the radius of the joint PrW , $R_{PrW} = 14.96 \cdot 10^{-3} m$.

6 Summary of appended papers

This thesis comprises three appended papers (Appendices **A-C**). Paper **A** gives the kinematical results together with important geometric constraints and recommendations. Paper **B** constitutes a basis for the dynamical modelling of the machine and emphasises the importance of performance of work in the geometrical constraints realized by constraint loads. Paper **C** presents the full dynamic model and gives examples of simulation output as well as a comparison of the lateral force between piston and cylinder liner.

7 Discussion, future research and conclusions

The research has been directed to constructing an analytical rigid body mechanical model which gives position, orientation, velocity, acceleration and prediction of internal contact loads for the components of the design concept of the axial piston type steam expander with wobble plate, Z-shaft and load bearing capacity in a cone-to-cone contact. The feasibility of expanding steam with such an expander has been investigated and was found promising since the optimal shaft speed closely matches a range of applications spanning from stationary small scale heat and power generation to different automotive applications. The favourable order of magnitude of internal contact loads indicate a potential for oil-free operation by means of proper design solutions, combined with proper selection of construction materials and surface coatings. The balancing of inertia achieved by configuration of geometrical parameters and by dead-weights upon the Z-shaft shows the ability to construct a completely balanced machine. The overall aim was to design and construct an oil-free physical demonstrator. This was done in a cap stone project during 2008-2009 at the Royal Institute of Technology. This is further discussed in chapter “4 Model” and chapter “8.7 Full scale expander demonstrator”. The result have also been utilized and partially verified by other students projects, discussed in chapter “8 Associated work”.

As stated in Paper C, possible future work could be divided into two categories: further model development and rig testing. As to further refining the model under a rigid-body assumption, the introduction of friction loads would be one interesting approach. Coupled with tribological rig testing to determine the coefficients of friction in the different bearing types (which are the physical realization of the joints) under different load scenarios, this would make the calculated dynamic motion of the model more accurate. This also points out yet another interesting extension of the further development of the rigid-body model: running simulations and collecting results for a force/torque-driven motion instead of the inverse dynamics approach. The results of such forward dynamics simulations could be considered to model the actual machine more closely, and to deepen the understanding of the distribution of constraint loads internal and external to the machine. Running forward dynamics simulations also gives us the opportunity to model the engine brake. As mentioned in the introductory section, finite element analysis (FEA) could be conducted on single components by applying the constraint and applied loads to the component, thus reducing the complexity of the finite element analysis. How such a simplification would affect the FEA results should be considered. As to the possible drawbacks of an axial piston machine with load bearing capacity in the cone-to-cone contact between the wobble plate and engine block, the contact is modelled as a point contact, which would be the case if at least one of the conical surfaces were crowned. Eventual wear would result in a line contact, however, thus constraining the wobble plate from lateral rotation and resulting in an over-determined configuration. An optimization algorithm and selection of objective

functions could be applied to the analytical rigid body model. This could aid the selection of design parameters, such as the radius to the cone-to-cone contact (which affect both the surface pressure in the cone-to-cone contact as well as the torque in ZW).

7.1 Conclusions

From this research it has been concluded that a modern compact small-scale steam engine should be feasible for vehicular traction or in a bottoming cycle, as well as in a stationary CHP application. The piston machine offers a suitable optimal shaft speed which removes the need for complex gearing and coupling. It is further more insensitive to erosion from droplets as compared to a turbine, and possibly more robust. The axial piston machine offers an almost unique possibility to greatly reduce the lateral force between piston and cylinder liner, thus reducing the pv-number in the only internal contact subjected to great sliding velocities. The possibility to carry a major part of the force exerted by the steam expansion in a rolling contact of large equivalent radius is also offered by the axial piston type configuration. There is a possibility to completely balance the inertia loads of the machine with proper configuration of some geometrical parameters and by means of dead-weights. Vibrations and noise would then be significantly reduced, hence extending the machines life span as well as making it more attractive to the end user and the surrounding environment. The axial piston configuration allows for one single centrally placed rotating valve with short inlet canals which allows for high rotational speed. A multi-cylinder engine gives smoother torque characteristics also at low rpm's.

8 Associated work

As mentioned in the introductory chapter several student projects (candidate and cap stone projects, and master thesis's) closely associated to the work presented in this thesis have been carried out. Work done have focused on the component or system design of the expander, simulations on and realization of valve prototype, test rig development, concept design on a bottoming cycle applied in a long-haul truck and on a small-scale solar power plant.

8.1 Rigid body MBS model

As a candidate project [18] in the 3rd year of the machine design education a rigid body model of the machine was created in the commercial MBS (Multi-Body Simulation) computer program ADAMS. The aim was to investigate the exportability to ADAMS of a parameterized CAD (Computer Aided Design) model of the expander in the commercial computer program Solid Edge. A further objective was to investigate the ability to realize a general coupling of the motion of the wobble plate and Z-shaft without introducing a net performance of mechanical work upon the system of rigid bodies.

From this study, some of the analytical results on geometry, kinematics and dynamics could be verified although differences in the modelling approach made such comparisons tedious. A model intended to optimize the design should be modelled directly in ADAMS since exporting CAD-models to ADAMS require a great amount of manual labour. The generic ADAMS joint “coupler” could be used to realize the generalized coupling of the motion of the Z-shaft and wobble plate.

8.2 Finite Element Analysis

Two studies have been conducted using finite element analysis, carried out as one 3rd year candidate project in machine design and one master’s thesis. The commercial computer program Ansys Workbench was used.

The first project [19] focused on evaluating the sensibility of the responses on surface pressure, von Mises stress, eigen frequencies, buckling load and stiffness from the general angle of tilt β of the piston rod, length of piston rod, the material’s Young’s modulus and the radius of the piston rod ball joint. This constituted a design of experiments study with four parameters, two levels and five responses. Some conclusions concerning the piston rod design were:

- decreasing contact pressure between piston rod and wobble plate with increased ball joint radius,
- decrease in bending stress follows decrease of β and friction coefficient in the contacts,
- increased first eigenfrequency with decreased piston rod length and ball joint radius,
- higher buckling load with decreased piston rod length,
- increased stiffness with decreased piston rod length and ball radius.

Recommended future work was to model a hydrostatic bearing and predict the contact pressure and stress distribution, and also to further investigate the role of thermal softening of the materials.

The master’s thesis conducted by Asplund [20] focused on modelling a mass optimized piston and piston rod (as a single component) and studying the wobble plate and the mechanical interfaces and their locations between piston rod and wobble plate and Z-shaft, engine block and wobble plate. The analytical results from the model presented in this licentiate thesis were used to perform FE-simulations of the individual components, and were also verified. Where possible, calculations of life time expectancy of the bearings were performed. Examples of conclusions were that if the piston rod’s diameter is dimensioned with a safety factor of 2 concerning buckling, it should be at least 13 millimetres in diameter. Further, the CARB type roller bearings from SKF seem suitable

as mechanical interfaces between wobble plate and Z-shaft due to the possibility of relative axial displacement between these two components.

8.3 Valve technology, simulations and prototypes

Two studies have been conducted to investigate possible valve designs and to design and construct a valve prototype. This study was carried out as one 3rd year candidate project in machine design followed by one 4th year machine design cap stone project.

The first project [21] focused on investigating different valve mechanisms such as cam-follower, rotating valves, electromechanical and pneumatic actuators. Further, a CFD-simulation (Computational Fluid Dynamics) was conducted to study the transient behaviour of the working media when opening a poppet valve to the cylinder. The study gives a basis to different valve techniques but concludes that the specific computed results rely on the design and parameter values and that the CFD results are unreliable. Recommendations are made to address the possibility of developing a pilot controlled valve.

The second project [22] continued with an in-depth investigation of different valve mechanisms. Following generation and evaluation of the most promising concepts, an electromechanical pressure balanced slide valve was selected. A cam profile could be used to open the valve since the valve opening time is dependent on the Z-shaft rotation only. The closing of the valve should follow the desired filling (“throttle”, cut-off, φ_{Fill}) and a solenoid was used as an actuator (Figure 27).

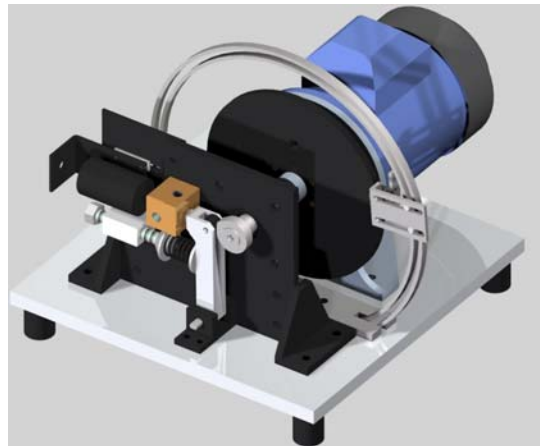


Figure 27 – CAD drawing of the valve prototype. The image depicts (among other) electric motor, cam and follower, slide valve housing (yellow cube) and solenoid (From [22]).

Opening times ranges from 0.4 ms to 0.4 s and the opening area was specified to 29 mm². A physical prototype was constructed and the functionality up to 1400 rpm and

down to $\varphi_{Fill} = 15^\circ$ (opening time 0.9 ms) was demonstrated with pressurized water at 120 bar (Figure 28). The leakage was about 4%.

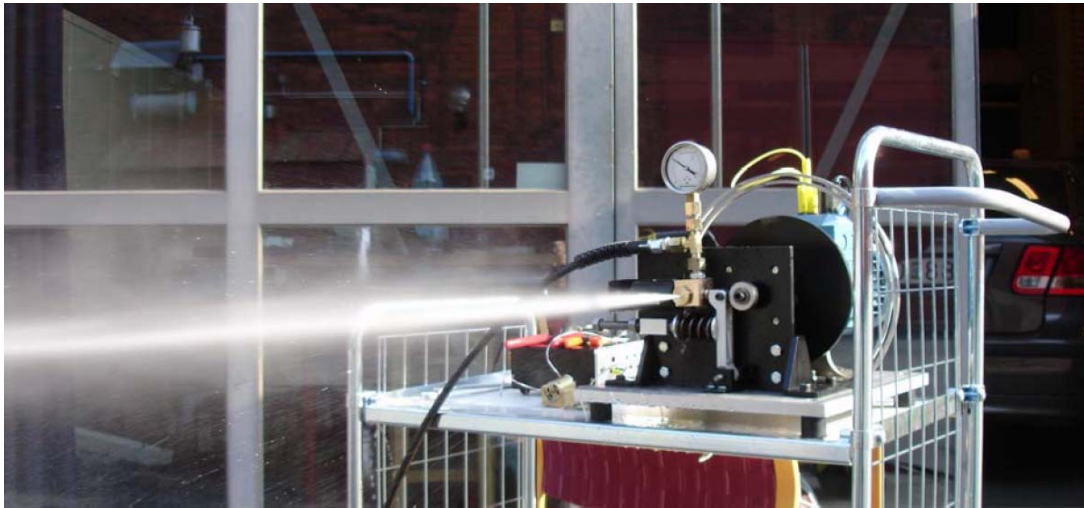


Figure 28 – The physical valve prototype (From [22]).

8.4 Hydrostatic lubricated seal

The master's thesis by Schjelderup [23] focused on designing and constructing a device to guide pressurized water from a foundation fixed source into the reciprocating piston rod and further into the piston with the purpose to hydrostatically separate the piston/piston ring and the cylinder liner surfaces (Figure 29). This was realized by constructing a device that embraced the piston rod with a water inlet (from the source) and a water outlet (into the piston rod and finally to the piston and piston ring).

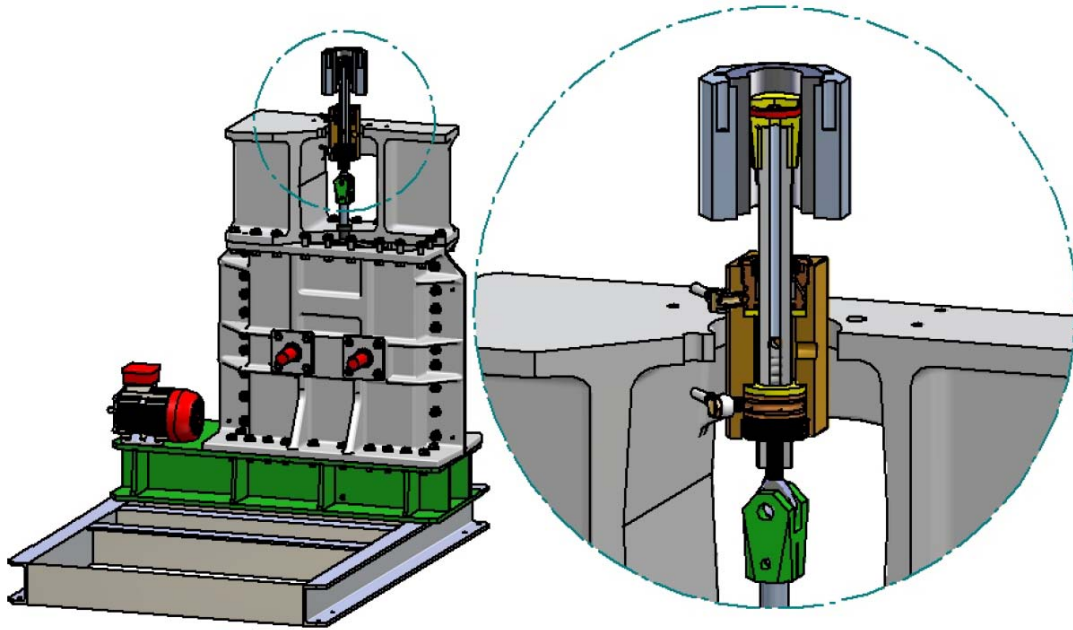


Figure 29 – The test rig depicting foundation, electric motor, piston rod, piston and cylinder head. The work done by Schjelderup [23] focused on improving and redesigning an existing test rig and designing and constructing the device embracing the piston rod with the purpose of conducting pressurized water from a fundament fixed source to the surface between piston and cylinder liner. The leftmost image depicts the test rig and the rightmost shows an enlargement of the embracing device (From [23]).

The aim of the project was met, i.e. a complete test rig was realized and prepared for piston ring tests (Figure 30).

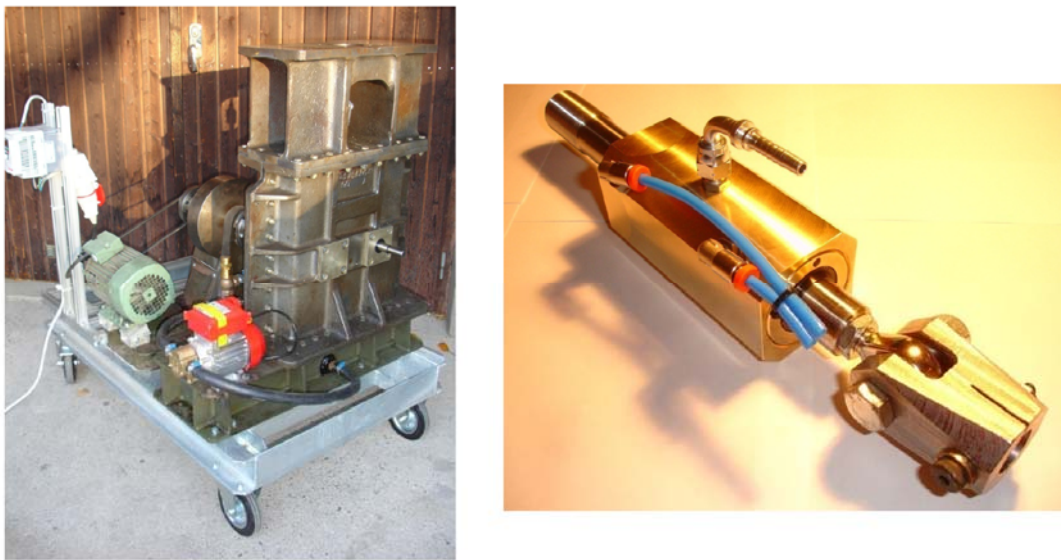


Figure 30 – The complete test rig (left image) and the embracing device (right image) (From [23]).

8.5 Bottoming cycle

A 3rd year candidate project [24] investigated the potential of and the possibility to realize a steam engine bottoming cycle in a long haul truck, connecting the steam generator directly to the diesel engines outlet manifold (Figure 31). An FE-analysis of thermo elastic stresses was also made on the exhaust manifold system. The study gives a basis to the required integral components of the system, giving an estimated weight of the steam generator package to 160 kg, and recommends further examining the expander and the air-cooled condenser system.

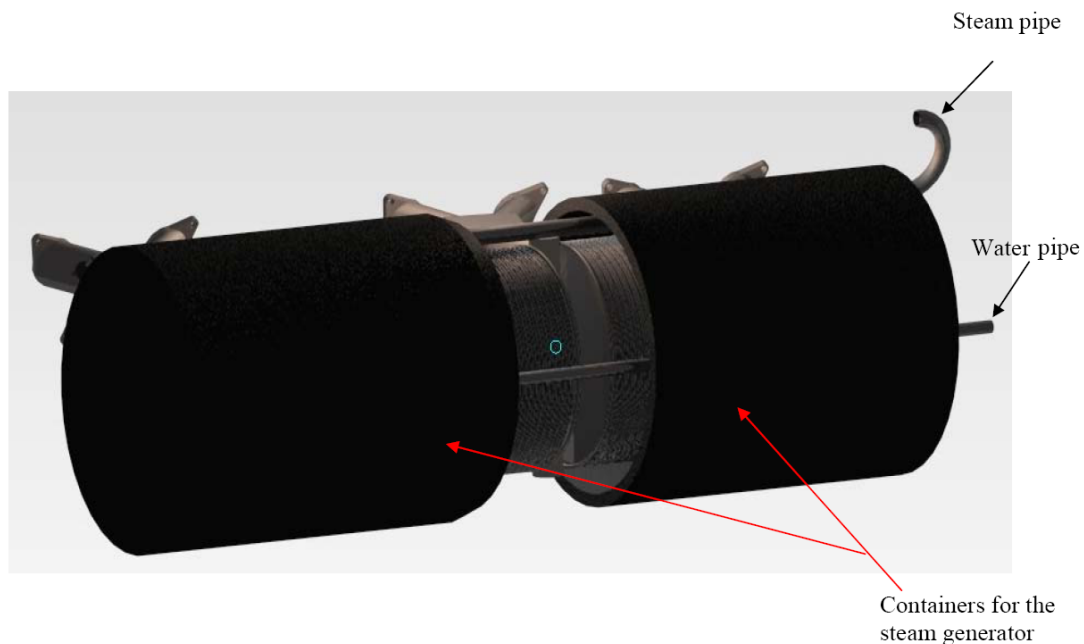


Figure 31 – An illustration of the steam generator package connected to the exhaust manifolds (seen in the upper part of the image) of a diesel engine (from [24]).

8.6 Small scale solar power plant

A 3rd year candidate project [25] was conducted concerning the possibility to realize a small-scale robust solar power plant. The aim was to investigate the possibility of collecting and focusing solar radiation in parabolic troughs, generating steam, and together with some buffer system (steam and or solid state buffer) expanding and generating electricity. This study gave recommendations on the integral components of the system and working media as well as estimations of sizes, power range and profile over the day and night.

8.7 Full scale expander demonstrator

As a 4th year machine design cap stone project [16] a full scale expander demonstrator was designed and constructed utilizing the result presented in this thesis. As mentioned in chapter 3 Model, the requirements from the first specifications of demands were not met which is thoroughly described in [16] as well as the vast amount of conclusions. The

machine was constructed in order to meet the actual requirements originating from it being subjected to 250 bar admission pressure in the cylinders. Thought was given to conceptual solutions to meeting the demands from the high temperature and oil-free drive or sealing of the crank mechanisms bearings from the cylinders in order to avoid oil-contamination of the working fluid. The Figure 32 and Figure 33 illustrate the drawings and the final demonstrator.

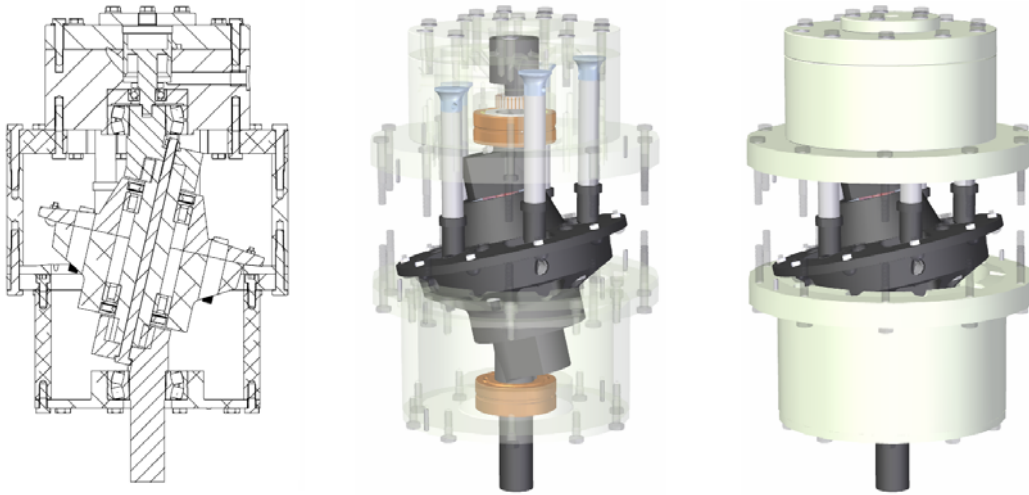


Figure 32 – CAD drawing and 3D renderings of the physical demonstrator of the axial piston type steam expander constructed in [16].



Figure 33 – The resulting physical demonstrator of the five-cylinder axial piston type steam expander constructed in [16].

References

- [1] Cengel, Y. A.. 1997, "Introduction to Thermodynamics and heat transfer", McGraw-Hill, United states of America.
- [2] Egnell, R., Gabrielsson, R., 1991, "Alternativa motorer" or "Alternative engines", NUTEK-info 829-1991, Stockholm, Sweden.
- [3] <http://www.microchap.info/>
- [4] Persson, J-G., November 2000, "Turbo vs' displacement type fluid machinery - characteristics and operating ranges", ICME '2000 First International Conference on Mechanical Engineering, Shanghai, China.
- [5] Platell, P., 1993, "Displacement expanders for small scale cogeneration", Licentiate thesis, Machine Design, Royal Institute of Technology, Stockholm, Sweden.
- [6] RANOTOR AB, 1993-11-01 – 1994-08-31, "Rapport över RAN-projektet" or "Report of the RAN-project", Nutek Diariennr 8522-93-12116, Stockholm, Sweden.
- [7] Persson, J-G., October 1990, "Performance mapping versus design parameters for screw compressors and other displacement compressor types". Schraubenmaschinen '90, VDI-Berichte 859, pp 15-31, VDI – Verein Deutsche Ingenieure, Dortmund, Germany.
- [8] Setright, L. J. K., 1975, "Some unusual engines", Mechanical Engineering Publications for the Institution of Mechanical Engineers, UK.
- [9] Chen, Y. 2006. "Novel cycles using carbon dioxide as working fluid", Department of Energy Technology, Royal Institute of Technology, Stockholm, Sweden.
- [10] Naqvi, R. "RAN Steam Buffer: Thermal Energy Storage in Porous Ceramic Media", Master thesis, Royal Institute of Technology, Stockholm, Sweden.
- [11] Platell P., December 1983, "Analys av de allmänna driftbetingelserna för en personbil samt bränsleförbrukning och prestanda för en bil försedd med ångmotorsystemet RAN" or "Analysis of the general load scenarios of a normal car and the performance of a car equipped with the steam engine system RAN", Master thesis, Thermal Engineering, Royal Institute of Technology, Stockholm, Sweden.
- [12] Lang, O. R., 1966 "Triebwerke schnellaufender Verbrennungsmotoren", Springer, pp. 9-14, Germany.
- [13] Changqing Tian, Chunpeng Dou, Xinjiang Yang and Xianting Li , 2004, "A mathematical model of variable displacement wobble plate compressor for automotive air conditioning system", Applied Thermal Engineering **24** (2004) 2467–2486.
- [14] Pedersen, N. L., December, 1997, "Optimization of the Rigid Body Mechanism in a Wobble Plate Compressor", Multibody System Dynamics Volume **1**, Number 4 / December, 1997.

- [15] Lesser, M., 1995, "The analysis of complex nonlinear mechanical systems, a computer assisted approach", World scientific series on nonlinear science Series A Vol. 7.
- [16] Granquist, D., Larsson, E., Olofsson, E., Strömberg, R., 2009, "Konstruktion av en femcylindrig axialkolvångmotor med vobbelmekanism" or "Design and construction of a five-cylinder axial piston type steam engine with wobble mechanism", Cap stone project report, Machine design, Royal Institute of Technology, Stockholm, Sweden.
- [17] Featherstone, R., 2007 "Rigid body dynamics algorithms," Springer; 1 edition (November 26, 2007), Germany.
- [18] Jonsson, J. and Granquist, D., 2008 "Simulering av en axialkolvmaskin – moderna ångmotorer" or "Simulation of a axial piston type engine – modern steam engines", Candidate thesis Machine Design, Royal Institute of Technology, Stockholm, Sweden
- [19] Jarl, J. and Olofsson, E., 2008 "Moderna ångmotorer – kolvstångens elastiska egenskaper" or "Modern steam engines – the elastic properties of the piston rod", Candidate thesis, Machine Design, Royal Institute of Technology, Stockholm, Sweden.
- [20] Asplund, D., 2008 "Konstruktionsstudie av en ångexpander" or "Construction study of a steam expander", Masters thesis, Machine Design, Royal Institute of Technology, Stockholm, Sweden.
- [21] Schjelderup, K. and Geiger, B., 2007 "Snabba ventiler" or "Quick valves", Candidate thesis, Machine Design, Royal Institute of Technology, Stockholm, Sweden.
- [22] Schjelderup, K., Asplund, D. and Nilsson, M., 2008 "Konstruktion av en ångventil – Utveckling och utvärdering av inloppsventil till en ångmotor" or "Construction of a steam valve – the engineering and evaluation of a steam engine inlet valve", Cap stone project report, Machine Design, Royal Institute of Technology, Stockholm, Sweden.
- [23] Schjelderup, K., 2008 "Konstruktion av testrigg för moderna ångexpandrar" or "Construction of a test rig for modern steam expanders", Masters thesis, Machine Design, Royal Institute of Technology, Stockholm, Sweden.
- [24] Solaka, H., 2007 "A novel steam engine concept", Candidate thesis, Machine Design, Royal Institute of Technology, Stockholm, Sweden.
- [25] Larsson, M., Söderberg, C. and Örning, C., 2009 "Småskaligt soldrivet ångkraftverk" or "Small scale solar powered steam power plant", Candidate thesis, Machine Design, Royal Institute of Technology, Stockholm, Sweden.